Bulletin of the Seismological Society of America, Vol. 94, No. 4, pp. 1207–1228, August 2004

Short-Term Properties of Earthquake Catalogs and Models of Earthquake Source

by Yan Y. Kagan

Abstract I review the short-term properties of earthquake catalogs, in particular the time and size distributions and the completeness of the early part of aftershock sequences for strong, shallow earthquakes. I determine the parameters of the Omori and Gutenberg–Richter laws for aftershocks close in time to a mainshock. Aftershock sequences of large earthquakes in southern California (1952 Kern County, 1992 Joshua Tree–Landers–Big Bear sequence, 1994 Northridge, and 1999 Hector Mine), recorded in the CalTech catalog, are analyzed to demonstrate that at the beginning of these series, many small earthquakes are absent from the catalog. The number of missing earthquakes increases with the magnitude range of a catalog and for some data sets exceeds the number of aftershocks close to a mainshock listed in a catalog. Comparing global earthquake catalogs (Harvard Centroid Moment Tensor and Preliminary Determination of Epicenter) with local data sets indicates that the catalogs based on longer period waves miss many early aftershocks even when their magnitudes are well above the stated magnitude threshold. Such short-term incompleteness may introduce significant biases to the statistical analysis of the seismicity pattern, in particular for branching models of earthquake occurrence incorporating the Omori law. For such models the likelihood function strongly depends on close aftershocks. I review the techniques to alleviate this problem. Analyzing the source rupture process of several recent large earthquakes suggests that rupture propagation is highly inhomogeneous in space, time, and focal mechanism. These random variations in the rupture process can be viewed as an extension of the aftershock stochastic generating mechanism toward the origin time of a mainshock. I review various models of the earthquake rupture process and suggest that fractal distributions of microevents in time, space, and focal mechanism constitute the development of an earthquake. The final identification of an individual earthquake depends on both objective and subjective factors.

Introduction

This article presents a quantitative, statistical analysis of short-term aftershock sequences, as recorded in local and global earthquake catalogs, and discusses how results of such analysis affect possible earthquake source properties. Historically, it is known that for various reasons aftershocks immediately following a strong, shallow mainshock are not completely registered (Omori, 1894; Utsu, 1969; Kagan, 1991b; Utsu *et al.*, 1995; Kisslinger, 1996; Narteau *et al.*, 2002). However, neither the properties of these close-in-time aftershocks nor the degree of the catalogs' nonuniformity have been studied systematically. For example, there are some indications that the degree of incompleteness varies for aftershocks of different size (Utsu *et al.* [1995], see their table 1 and figure 2; Wiemer and Katsumata [1999]; Narteau *et al.* [2002], their tables 2–4), but no specific investigation of this effect has been carried out.

Why pursue these investigations now?

- Although stochastic models of earthquake occurrence employing a power-law temporal aftershock decay have been used for a long time (Kagan and Knopoff, 1980, 1987b; Ogata, 1988, 1998, 1999), there is now widespread interest in applying such models (Console and Murru, 2001; Felzer *et al.*, 2002, Gerstenberger *et al.*, 2002; Helmstetter and Sornette, 2002; Sornette and Helmstetter, 2002). There is also increased interest in statistical analysis of seismicity using likelihood methods. The results of such likelihood analysis are used to evaluate and forecast time-dependent earthquake probability. The value of the likelihood function depends primarily on the earthquake rate immediately following a strong event (Kagan, 1991b). If the catalog incompleteness depends on the aftershock magnitude, this

relationship may also introduce systematic errors in the likelihood procedure. Hence, to obtain an unbiased result, one needs to know the short-term properties of a catalog.

- The behavior of aftershock sequences during the first minutes and hours is a significant component of theoretical models of seismicity (Dieterich, 1994; Kisslinger, 1996; Madariaga and Olsen, 2002; Narteau *et al.*, 2002; Rubin, 2002). The major issue in such a development is whether the coefficient c in the Omori law (see equation 1) is a physical parameter, that is, is independent of methods of registration and interpretation of a seismogram, or if it simply indicates a measure of instrument and technique deficiency. A more complete understanding of aftershock generation may thus serve as a model validation tool.
- Improved seismic and geodetic instrumentation, new methods of interpretation, and a strong increase in computer power have enabled us to obtain a detailed time-space picture of the rupture process for several large earthquakes. For instance, special issues of the *Bulletin of the Seismological Society of America* (*BSSA*) have been dedicated to the Loma Prieta, Landers, and Northridge, California; Chi-Chi, Taiwan; Izmit, Turkey; and Hector Mine, California, earthquakes. These studies revealed a complex rupture history. Such factors as the spatially varying slip distribution, complex fault geometry, and temporal delays during rupture may be seen as extrapolating short-term aftershock behavior to the origin time of a mainshock. Comparing results on the rupture time history with short-term aftershock distributions calls into question the usual representation and models of earthquake source.

In this work I first investigate several aftershock sequences in southern California and then short-term earthquake properties in two global catalogs (the Harvard Centroid Moment Tensor [CMT] and the Preliminary Determination of Epicenter [PDE]). Next the results of these statistical studies are compared to different models of the earthquake process, such as a stochastic point process, representations involving extended earthquake source properties, an earthquake source consisting of subevents with the power-law size distribution, and finally a fractal source model.

Aftershocks and Their Approximations

Two statistical regularities are commonly invoked in studying aftershock distributions: the Omori law of aftershock temporal occurrence rate (Utsu *et al.*, 1995) and the Gutenberg–Richter (G–R) relation (Utsu, 1999, 2002) for their magnitude distribution. Hundreds of papers have been published on these laws since their discovery by Omori (1894) and Gutenberg and Richter (1941, 1944). Short-term aftershocks deviate from these laws due to the specifics of registration and interpretation, as well as the properties of the earthquake source process. To study deviations in these laws, we need first to discuss a methodology.

Aftershock Temporal Behavior

Omori (1894) proposed the formula for aftershock rate decay in time (t):

$$n(t) = \frac{K}{t + c}, \tag{1}$$

where K and c are coefficients and $n(t)$ is the aftershock frequency measured over a certain interval of time (∂t or Δt). Extensive investigations (Utsu [2002] and references therein) have shown that equation (1) is a reasonable approximation for many aftershock sequences. Rubin (2002) demonstrated that the Omori law is valid even for stacking aftershock sequences of microearthquakes.

Presently a more complicated equation approximates the aftershock sequence numbers:

$$n(t) = \frac{K}{(t + c)^p}, \tag{2}$$

and it is called the "modified Omori formula" (Utsu, 1961, 1969; Utsu *et al.*, 1995). Aftershocks often display secondary, tertiary, and so on, clustering, that is, strong aftershocks have their own sequence of dependent events. Therefore, the fit of aftershock numbers by equations (1) and (2) is often unsatisfactory (Utsu *et al.*, 1995).

To explain an earthquake occurrence in complex aftershock sequences, as well as the foreshock/mainshock pattern and background seismicity, stochastic point models have been proposed over the years. The formula (equation 2) is incorporated in the epidemic-type aftershock sequence models by Ogata (1988, 1998). The p coefficient value should be larger than 1.0 in the stochastic process models, since each shock is assumed to be a potential source of finite numbers of dependent events. Kagan and Knopoff (1987b), Kagan (1991b), and Kagan and Jackson (2000) used a simpler formula with the coefficient $c = 0$, but they removed closeby aftershocks from the catalog (see equation 18) and made appropriate adjustments in the likelihood procedure (see more details in Kagan [1991b]).

Ogata (1983) proposed a maximum likelihood algorithm and a FORTRAN program to evaluate the parameters of equation (2) and estimate their statistical uncertainties. Ogata (1983, 1999) suggested using an additional parameter, T_s, the beginning of the time interval where equations (1) and (2) are valid. Utsu *et al.* (1995) and Utsu (2002) reviewed the results of several studies of aftershock sequences using the modified Omori formula and Ogata method.

This work considers only the early parts of aftershock sequences where the aftershock numbers, especially in the very beginning of a sequence, are relatively small. I employ a robust procedure to approximate the aftershock rate decay. For such purposes I use the original Omori equation (equation 1), but instead of using the time interval (t) between the mainshock and an aftershock, I take its natural logarithm

$\tau = \log t$ as input for plotting and analysis. Hence I count aftershock numbers in logarithmic time intervals ($\partial\tau$ or $\Delta\tau$). The advantage of τ is that, for the time intervals much larger than c, the aftershock numbers in equation (1) would be uniform. In contrast, equations (1) and (2) anticipate that the number of aftershocks in linear time intervals is uniform as one approaches the mainshock origin time ($t \to 0$), but that proposition is not justified on observational grounds (see Fig. 3). For time close to $t = 0$, the aftershock rate behavior is seen more clearly with logarithmic time intervals than with linear bins, where their variations are smoothed due to the large number of events in time intervals used.

If aftershocks are observed over a time interval $t_1 - t_2$, we obtain the following statistical distribution:

$$\phi(\tau) = A^{-1} \times \frac{e^{\tau}}{e^{\tau} + c}, \tag{3}$$

where

$$A = \log \frac{t_2 + c}{t_1 + c} \tag{4}$$

is the normalization coefficient and ϕ is the probability density function (pdf). The average logarithmic interval is

$$\bar{\tau} = \int_{\tau_1}^{\tau_2} \tau\phi(\tau)\partial\tau = A^{-1}\left[\tau_2 \log \frac{t_2 + c}{c} + \mathrm{Li}_2\left(-\frac{t_2}{c}\right) - \tau_1 \log \frac{t_1 + c}{c} - \mathrm{Li}_2\left(-\frac{t_1}{c}\right)\right], \tag{5}$$

where $\tau_i = \log t_i$ and Li_2 is the dilogarithm function (Abramowitz and Stegun, 1972; Prudnikov *et al.*, 1992). Higher-order statistical moments of equation (3) can be obtained using symbolic manipulation programs like Mathematica (Wolfram, 1999); they can also be expressed by polylogarithms, Li_n, and can numerically be estimated by Mathematica. The standard deviation for the logarithmic time interval, σ_τ, is

$$\sigma_\tau = \left(\int_{\tau_1}^{\tau_2} \tau^2\phi(\tau)\partial\tau - \bar{\tau}^2\right)^{1/2}. \tag{6}$$

The empirical logarithmic moments (average and standard deviation) can easily be calculated for aftershock sequences:

$$\tilde{\tau} = \frac{1}{n}\sum_{j=1}^{n} \log t_j \tag{7}$$

and

$$\tilde{\sigma}_\tau = \left[\frac{n}{n-1}\left(\frac{1}{n}\sum_{j=1}^{n}(\log t_j)^2 - \tilde{\tau}^2\right)\right]^{1/2}, \tag{8}$$

where n is the number of aftershocks in a sequence.

These empirical statistical moments can be used to approximate the aftershock distribution. One possibility is to use the Omori law in its logarithmic form (equations 3–4) but then apply equation (5) and a similar, more complicated expression for σ_τ to evaluate the c coefficient. Figure 1 displays the dependence of $\bar{\tau}$ and σ_τ on c. I use $t_1 = 0.0001$ days and $t_2 = 128$ days. From the display, it is obvious that for $t_2 \gg c \gg t_1$ the dependence can be approximated by the formula

$$c' \approx 10^{0.93\bar{\tau} - 1.97} \text{ or } c'' \approx 10^{3.27 - 1.76\sigma_\tau}. \tag{9}$$

If aftershocks follow the Omori law (equation 3) exactly, both c estimates would be equal, that is, $c' = c''$.

Another possibility is to approximate the aftershock numbers in logarithmically increasing time intervals by a uniform (rectangular) distribution. In this case we expect the distribution to start at τ_0 (the effective beginning time for an aftershock sequence). Thus, an aftershock sequence is assumed to continue from time t_0 to time t_2 with the uniform rate, and the pdf

$$\phi(\tau) = \frac{1}{\tau_2 - \tau_0}. \tag{10}$$

This rate would be close to equation (3) for larger time intervals. For the uniform distribution over the interval $\tau_2 - \tau_0$, the average time and the standard deviation are

$$\bar{\tau} = \frac{1}{2}(\tau_2 - \tau_0') \text{ and } \sigma_\tau = \frac{1}{\sqrt{12}}(\tau_2 - \tau_0''). \tag{11}$$

Using these expressions, we can calculate the effective beginning time, τ_0, if statistical estimates of $\bar{\tau}$ or σ_τ are obtained from equations (7) and (8).

If aftershocks follow the uniform distribution exactly, the estimate is $\tau_0' = \tau_0''$. However, since this approximation is almost never exact, generally, it is $\tau_0' \neq \tau_0''$. Hence the difference in τ_0' versus τ_0'' gives some measure of uncertainty in the approximation. Later I use a geometric mean of two values,

$$\tau_0 = \sqrt{\tau_0'\tau_0''}, \tag{12}$$

to estimate the effective beginning time of an aftershock sequence.

Figure 2 shows the values of τ_0' and τ_0'' one obtains if the aftershocks follow the Omori law (equations 3–4), but their distribution is modeled by the uniform law (equation 10). Clearly τ_0, especially τ_0', is a reasonably good estimate of the c value. Moreover, by the logarithmic transformation of time, I avoid using the T_s parameter (Ogata, 1983; Utsu

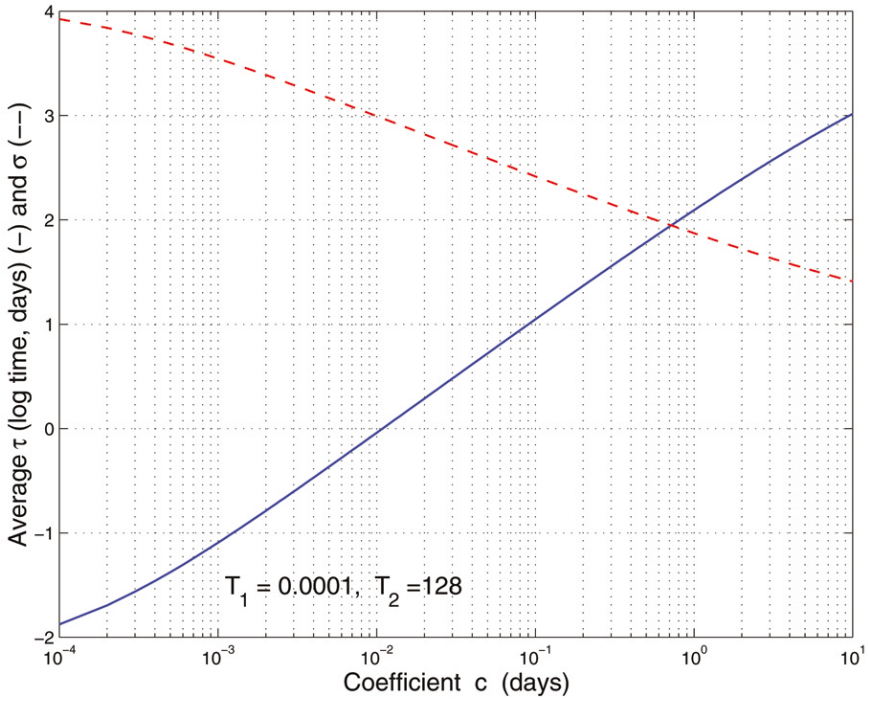

Figure 1. Dependence of logarithmic statistical moments (average, $\bar{\tau}$, and standard deviation, σ_τ) on the coefficient c for Omori law decay of aftershock numbers. Solid line is $\bar{\tau}$, dashed line σ_τ. Aftershock sequence is observed in time interval 0.0001–128 days.

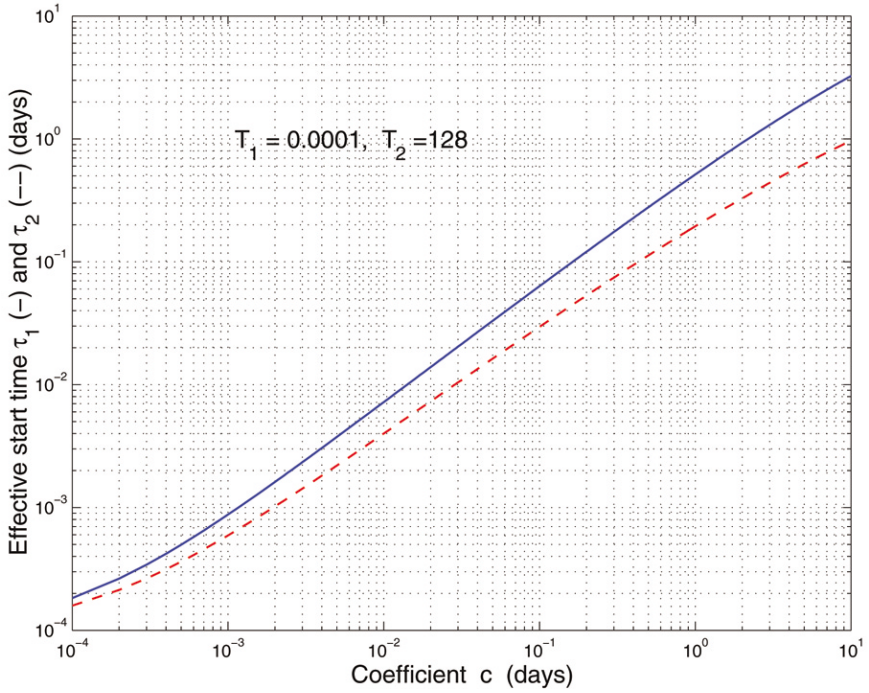

Figure 2. Dependence of effective beginning time for an aftershock sequence following the Omori law with coefficient c. Solid line is τ_0', estimated using logarithmic average time $\bar{\tau}$. Dashed line is τ_0'', estimated using σ_τ. Aftershock sequence is observed in time interval 0.0001–128 days.

et al. 1995), since it, as well as the c parameter, is incorporated in the beginning time, τ_0. Therefore the logarithmic transformation of time (equation 3) and the logarithmically uniform distribution of events (equation 10) have clear advantages in statistical analysis of short-term aftershocks: a smaller number of adjustable parameters that are estimated by a simple statistical moment method (equations 7–8), obviating the necessity for the complex Fletcher–Powell maximum likelihood search (Ogata, 1983).

Figure 3 is an example of aftershock sequence approximation for four types of estimates (equations 9–11). Circles are used for the numbers of aftershocks $2.4 \geq M \geq 2.0$ for the first 128 days following the 1992 Landers, California, earthquake. The aftershock numbers are counted for time bins decreasing by a factor of 2, so the values of $\tilde{\tau}$ and $\tilde{\sigma}_\tau$ in equations (7)–(8) need to be multiplied by log 2. Four approximations are shown: two for the Omori law (equation 9) and two for the logarithmically uniform distribution (equations 10–12). Since logarithmically decreasing time intervals are used, the numbers decay to zero for $t \to 0$. In the regular Omori law (equation 1) the time bins are linear (Δt). Equation (1) anticipates that the aftershock numbers continue to increase as $t \to 0$.

For longer time bins, aftershock numbers are the same (i.e., approximately uniform), but the numbers decrease for time intervals of less than 16 days. Neither the Omori law nor the uniform distribution fits the number decay well. Later I will discuss the reasons for the aftershock number shortage at small time intervals. The values of coefficients c and τ_0 based on $\tilde{\tau}$ and $\tilde{\sigma}_\tau$ are reasonably close.

Size Distribution of Aftershocks

The earthquake size distribution is commonly described by the G–R magnitude–frequency relation (Gutenberg and Richter 1941, 1944),

$$\log_{10} n(M) = a - bM, \tag{13}$$

where $n(M)$ is the number of earthquakes with magnitude $\geq M$ and a and b are parameters: a characterizes seismic activity or earthquake productivity of a region and b describes the relation between small and large earthquake numbers, $b \approx 1$.

Given the limited sensitivity of seismographic networks, small earthquakes are not completely sampled in earthquake catalogs. This makes it necessary to introduce a catalog completeness threshold (observational cutoff) M_t and truncate the distribution from the left:

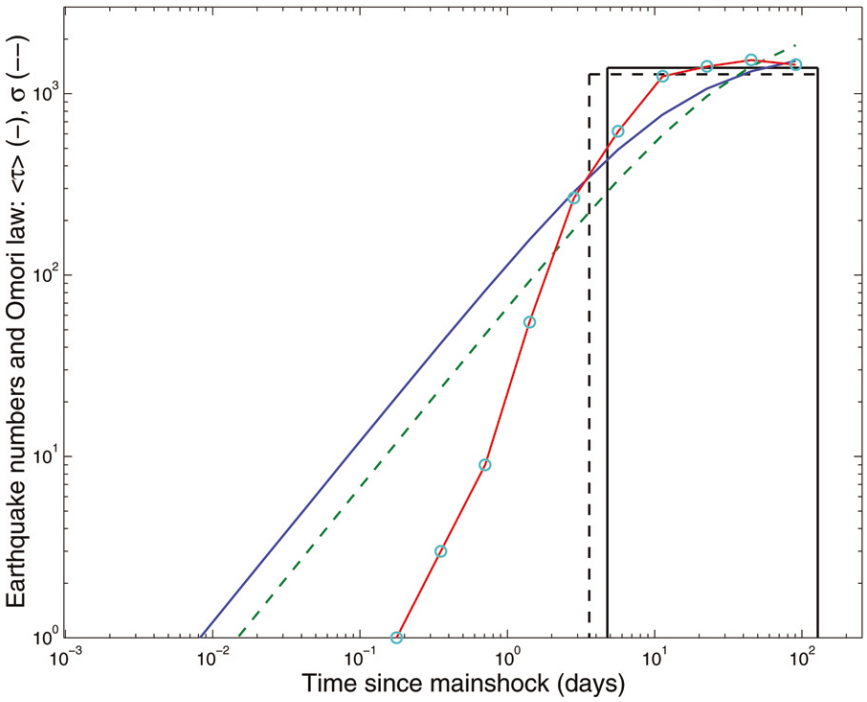

Figure 3. Distribution of aftershock numbers for the 1992 Landers, California, mainshock. Aftershocks in magnitude range $2.4 \geq M \geq 2.0$ are selected in spatial window latitude 33.5°–36.0° N, longitude 116.0°–118.0° W and are shown by circles. Aftershock sequence is observed in a time interval ending at 128 days after the mainshock. They are counted in time intervals increasing by a factor of 2. Four approximations are shown: two for the Omori law and two for the logarithmically uniform distribution (rectangular plots). Solid lines are the estimates based on the average logarithmic time ($\tilde{\tau}$); for dashed lines $\tilde{\sigma}_\tau$ is used.

$$\log_{10} n(M) = a_t - b(M - M_t) \text{ for } M_t \le M, \quad (14)$$

where a_t is the logarithm of the number of earthquakes with $M \ge M_t$.

The b-value can be estimated by the maximum likelihood method (Utsu, 2002):

$$b = [(\bar{M} - M_t + 0.05) \times \log(10.0)]^{-1}, \quad (15)$$

where $\bar{M}$ is the mean magnitude of earthquakes $M \ge M_t - 0.05$. The expression assumes that magnitudes are rounded off to the closest 0.1 value; thus 0.05 is the correction for magnitude discretization (Utsu [2002], his equation 16). The standard error is $b/\sqrt{n}$.

The magnitude threshold is most frequently estimated by comparing the magnitude–frequency plot with the G–R relation to see when the observational curve significantly differs from the theoretical law (equation 14) for small earthquakes (Wiemer and Wyss, 2000; Kagan, 2003). Earthquakes below the threshold are normally removed from a catalog before its statistical analysis. Unfortunately, such a method for accurate threshold determination requires (1) that at least several tens or hundreds of earthquakes be available for analysis and (2) that earthquakes above the threshold follow the G–R relation exactly. Short-term aftershocks rarely meet these conditions. The number of aftershocks in the immediate wake of a mainshock is often small, and in many catalogs a reported magnitude exhibits many biases and nonlinearities (Kagan, 2003), which make applying the G–R law problematic.

Catalogs

The CalTech (CIT) data set (Hileman *et al.*, 1973; Hutton and Jones, 1993) was the first instrumental local catalog to include small earthquakes ($M \ge 3$), beginning in 1932. In recent years even smaller earthquakes have been included in the catalog. Presently the magnitude threshold is about 1.5 (Wiemer and Wyss, 2000).

The PDE worldwide catalog is published by the U.S. Geological Survey; the catalog available at the time this article was written ended on 1 January 2001. The catalog measures earthquake size, using several magnitude scales, and provides the body-wave (m_b) and surface-wave (M_S) magnitudes for most moderate and large events since 1965 and 1968, respectively. The catalog contains more than 50,000 shallow earthquakes with $m_b \ge 5$ from 1965 to 2001.

I study the earthquake distributions for the global CMT catalog of moment tensor inversions compiled by the Harvard group (Ekström *et al.*, 2003). The catalog contains more than 14,000 shallow earthquakes in a time period 1 January 1977 to 1 January 2002. Of these, 4096 events have moment magnitude $M_w \ge 5.8$ (see equation 20).

California Earthquakes

This section analyzes several southern California aftershock sequences of large earthquakes. The two largest California earthquakes of the twentieth century are among them: the 21 July 1952 Kern County and 28 June 1992 Landers events, as well as 23 April 1992 Joshua Tree, 17 January 1994 Northridge, and 16 October 1999 Hector Mine, recorded in the CIT catalog.

Temporal Distributions

Figure 4 displays the aftershocks of the 1952 M 7.5 Kern County earthquake in the first 2048 days of the sequence. It is obvious that whereas $M \ge 4.5$ aftershocks are distributed almost uniformly over log time, for the first 4 months after the mainshock, $M < 4$ events are almost all missing from the list. Richter (1955, p. 197) remarked that "listing is certainly incomplete for the first few hours on July 21. . . . Many shocks of magnitude over 4.0 must have escaped attention immediately following larger ones." From Figure 4 I conclude that although the CIT catalog is generally complete in the early years up to $M \ge 3$ (Hileman *et al.*, 1973), in the aftershock zone of the Kern County earthquake, the magnitude threshold was significantly higher for the first few months after the earthquake. The catalog is reasonably complete for $M \ge 3$ earthquakes outside the source region of that earthquake even during the initial part of the aftershock sequence.

Several factors may explain the weak aftershocks' absence from our records. In addition to the influence of larger aftershocks mentioned by Richter, general overlapping of the seismic records makes identification and location of many shocks difficult. Moreover, the seismographic network usually undergoes significant change in the wake of a strong event: some stations may be damaged during shaking, and temporary and new permanent stations are installed in the first days after a strong shock. If the magnitude range (ΔM) of a catalog is large, the earthquake rate increases by several orders of magnitude following a strong shock. This and workforce limitations contribute to a significant inhomogeneity in earthquake catalogs for close-in-time aftershocks.

Timescales of these factors vary. Whereas administrative and seismographic network changes require hours and days to accomplish, seismic signal overlapping depends both on record frequency range and the rate of aftershock occurrence. These latter effects should have a timescale on the order of seconds and minutes. Rubin (2002) showed that microearthquakes also display a down time of a few tens of seconds following a mainshock, when the significant number of aftershocks is missing.

Since the factors contributing to aftershock record inhomogeneity are at least partly human related and depend on such details of registration as the number of seismographic stations in an earthquake focal area, one should not expect strict regularity in these patterns. This irregularity is obvious in Figure 5, showing an aftershock distribution of

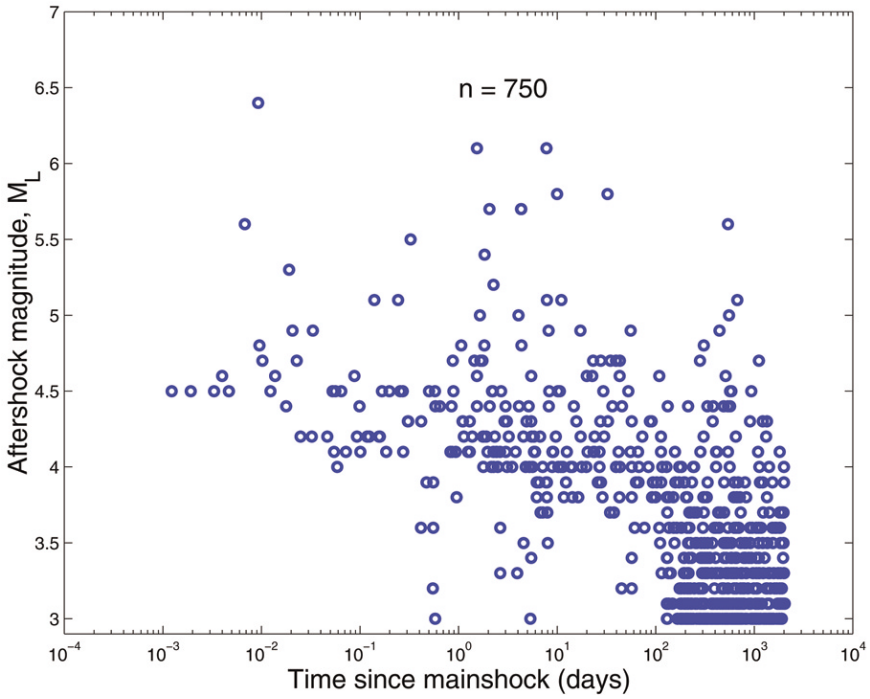

Figure 4. Time–magnitude distribution of 1952 *M* 7.5 Kern County, California, aftershocks. The window of latitude 34.8°–35.6° N, longitude 118.3°–119.3° W is used; the time interval is 2048 days after the mainshock.

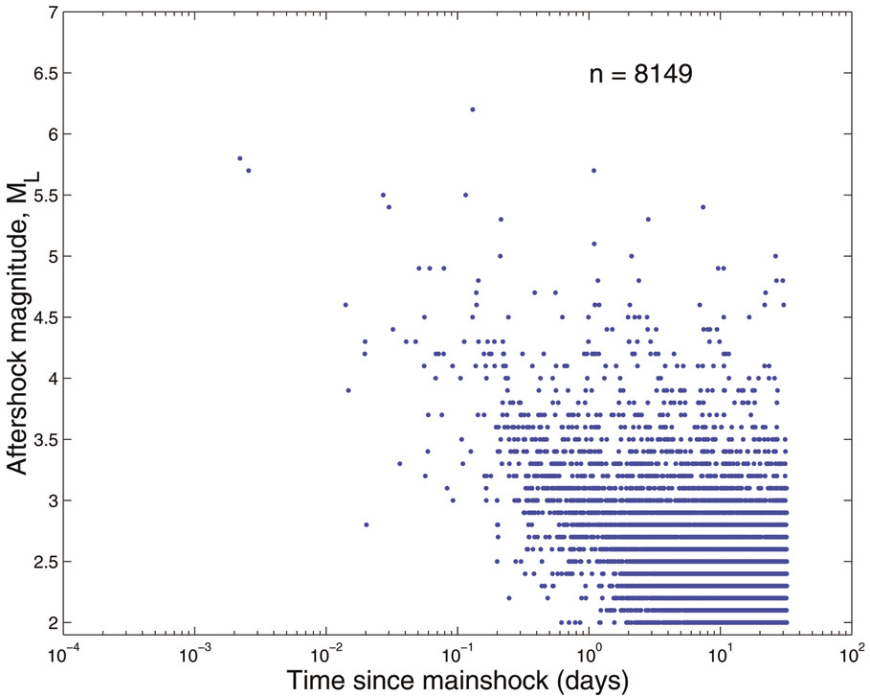

Figure 5. Time–magnitude distribution of 1992 *M* 7.3 Landers, California, aftershocks. The window of latitude 33.5°–36.0° N, longitude 116.0°–118.0° W is used; the time interval is 32 days after the mainshock.

the 1992 Landers earthquake. The general time–magnitude pattern is the same as for the Kern County events (Fig. 4): larger aftershocks begin early in the sequence, whereas the occurrence rate is progressively delayed for weaker events. Due to improved seismographic network capabilities and the computer availability for processing data, the delay in weaker aftershock registration is much smaller for the Landers event than for the Kern County earthquake.

The increased delay time for smaller aftershocks is observed not only for mainshocks. The strong (M 6.5) Big Bear aftershock, which occurred more than 3 hr after the Landers event, had aftershocks of its own (I used the window of latitude 33.9°–34.4° N, longitude 116.6°–117.2° W). These aftershocks behaved similarly to those in Figure 5.

In Figure 6 I show aftershock numbers for the 1994 Northridge, California, earthquake, as recorded in the local (CIT) and two global catalogs (PDE and CMT) for the first 32 days after the earthquake. The total number of CIT aftershocks is 25, whereas only 9 events are present in the PDE list. Although the magnitude threshold of the PDE catalog is likely to be close to 4.5 in southern California, several early aftershocks shown in the CIT catalog are not reported in the PDE list. Some missing short-term CIT aftershocks have $M \geq 5$, that is, well above the PDE magnitude cutoff. These events most likely are underreported as global network seismograms are of lower frequency. Since strong earthquakes have longer lasting long-period coda waves, it is more difficult to separate aftershocks and obtain their parameters.

A similar explanation can be supplied for the smaller number of aftershocks in the CMT catalog compared to the PDE list. The CMT catalog uses seismogram records with a period of a few tens of seconds (Dziewonski *et al.*, 1981), so a solution cannot be obtained for aftershocks closely following another large earthquake.

Kagan (1991a, 2003) noted significantly different numbers of aftershocks in various catalogs for the 1971 San Fernando (California) and the 1999 Chi-Chi (Taiwan) earthquakes. Table 3 in Kagan (2003) demonstrated that the shortest interearthquake time interval in catalogs depends strongly on seismogram frequency and methods of seismic record interpretation.

Figure 7 shows the numbers of aftershocks for the 1999 M 7.1 Hector Mine, California, earthquake as they depend on time interval and magnitude range (ΔM). The numbers demonstrate a similar relation: for time intervals longer than the c value, the distribution is approximately uniform, hence they follow the Omori law (equation 3). For smaller time intervals the numbers decay to zero. Similarly, as we see in the displays of Figures 4 and 5, stronger aftershocks have a smaller c value. Narteau *et al.* (2002, their tables 2 and 4) obtained a similar result: a decline of the c value with magnitude threshold increase when approximating the aftershock rate of the Hector Mine earthquake with the Omori law. Note

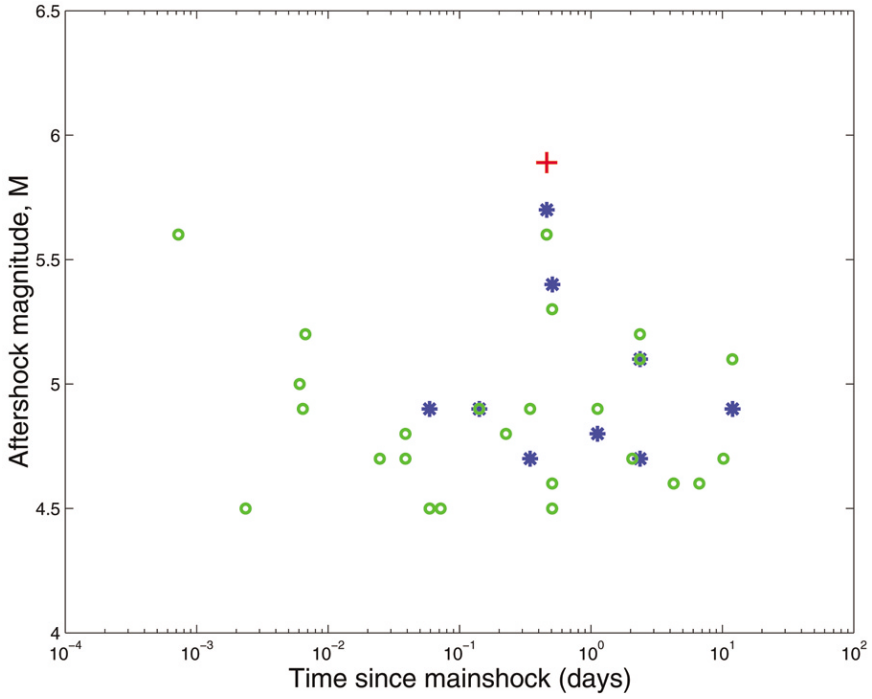

Figure 6. Time–magnitude distribution of 1992 M 6.7 Northridge, California, aftershocks. The window of latitude 34.0°–34.5° N, longitude 118.35°–118.80° W is used; the time interval is 32 days after the mainshock. Circles, aftershocks $M_L \geq 4.5$ from the CIT catalog; stars, aftershocks $m_b \geq 4.5$ from the PDE catalog; plus, aftershock from the CMT catalog.

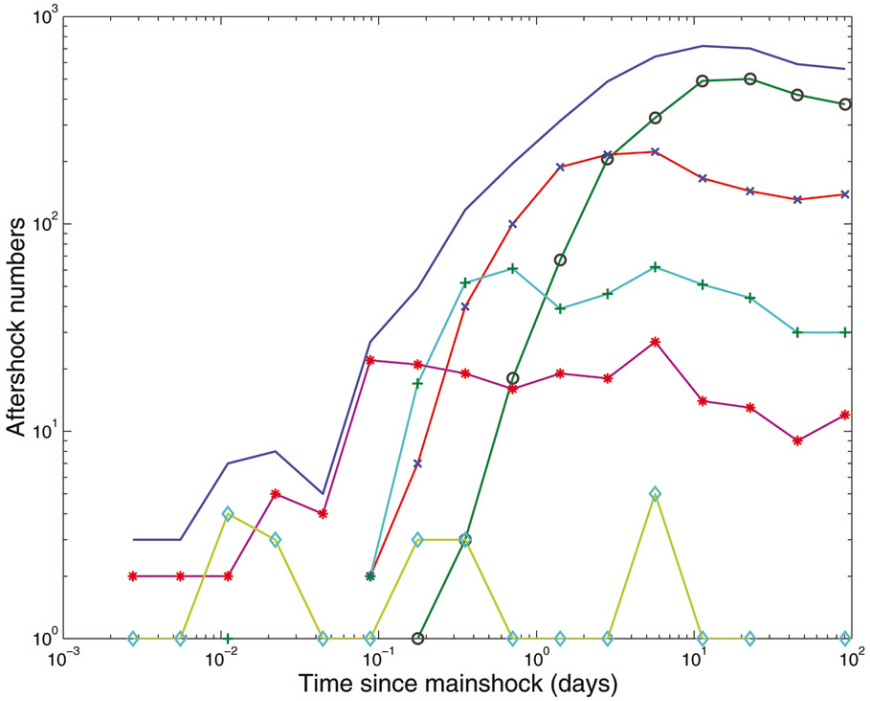

Figure 7. Aftershock numbers of the 1999 M 7.1 Hector Mine, California, earthquake. The window of latitude 34.0°–35.0° N, longitude 116.0°–116.5° W is used; the time interval is 128 days after the mainshock. Solid line, all aftershocks, $n = 4433$; circles, aftershocks $2.4 \geq M \geq 2.0$, $n = 2409$; crosses, aftershocks $2.9 \geq M \geq 2.5$, $n = 1356$; pluses, aftershocks $3.4 \geq M \geq 3.0$, $n = 435$; stars, aftershocks $4.4 \geq M \geq 3.5$, $n = 205$; diamonds, aftershocks $M > 4.5$, $n = 28$.

that if aftershocks in a narrow magnitude range follow the Omori law exactly, their sum (solid line in Fig. 7) cannot satisfy this relation, since it is a mix of several distributions with different c values.

I do not show error bars for the aftershock numbers displayed in Figure 7, since this would overload the diagrams. These uncertainties can be calculated according to the Poisson process, that is, proportional to $\sqrt{n}$. However, as Kagan and Jackson (2000, their figure 6) argued, due to earthquake clustering, the real uncertainties follow the negative-binomial distribution, which has larger error bars than the Poisson distribution. For annual time intervals, Kagan and Jackson (2000) found that the negative-binomial standard error is higher by about a factor of 2 than that for the Poisson law. For smaller time intervals as shown in Figure 7, the difference should be significantly higher.

In Figure 8 I show the dependence of the effective starting time τ on the aftershock magnitude range. This parameter was calculated similarly as in Figure 3 (see equations 11 and 12). Obviously, the large aftershocks start early in the sequence.

In this figure I also show two time limits, which may be useful in interpreting the results. One limit is time, t_r, for an earthquake to rupture through the focal zone. If we assume the rupture velocity $v = 1.5$ km/sec, the size of the earthquake source 1 km for the M 4 earthquake, and the source scaling relation

$$L \propto M_0^{1/3}, \tag{16}$$

where L is the source dimension and M_0 is the seismic moment of an earthquake (Kagan, 2002), then for unilateral rupture propagation

$$t_r = \frac{2}{3} \times 10^{(M-4)/2}, \tag{17}$$

in seconds.

The second limit, shown in Figure 8 is the magnitude-dependent time interval t_M employed by Kagan (1991b) to remove close-by aftershocks from a catalog to ensure its homogeneity:

$$t_M = 300 \times 10^{(M-4)/2}, \tag{18}$$

in seconds. In this expression it is assumed that coda waves of M 4 earthquakes last 300 sec.

The t_M limit was established by inspecting earthquake catalogs available at that time (Kagan, 1991b). These catalogs had a limited magnitude range of $\Delta M = 2.0$–3.7 (Ka-

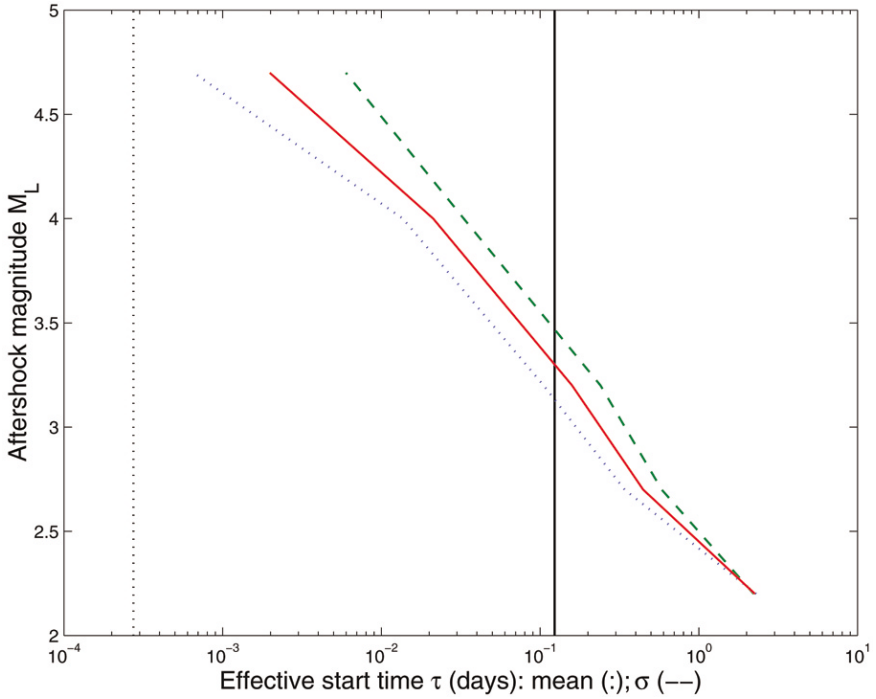

Figure 8. Effective starting time τ for aftershocks of the 1999 M 7.1 Hector Mine, California, earthquake. Solid line, τ_0; dotted line, τ_0'; dashed line, τ_0'', see equation (11). Vertical lines correspond to t_r (dotted line) and t_M (solid line) time limits; see equations (17) and (18). Both limits are calculated for the Hector Mine earthquake.

gan, 1991b, his table 1). For the Hector Mine (M 7.1) earthquake the t_M time limit seems satisfactory for aftershocks greater than M 4, that is, with a magnitude range on the order of 3.0.

Figure 9 displays the effective beginning time τ_0 for six large southern California earthquakes. The τ_0 parameter depends on the magnitudes of the mainshock and aftershocks: it increases with the mainshock magnitude but decreases with the aftershock magnitude. Both of these regularities can easily be explained: larger mainshocks have longer coda and a larger number of aftershocks. Therefore, the overlapping of earthquake records is more likely to occur. Larger aftershocks, on the other hand, have a better chance to be selected and processed from a complex record. Early $M \leq 4$ aftershocks of the Kern County earthquake may not have been processed deliberately; $M > 4$ aftershocks follow the pattern exhibited by the aftershocks of other large events.

From Figure 9 the dependence of τ_0 on the aftershock magnitude M_a can be approximated by an expression

$$\tau_0 \approx 10^{M_m - M_a - 4} \text{ days}, \qquad (19)$$

where M_m is the mainshock magnitude.

Reasenberg and Jones (1989, 1994) investigated aftershock sequences of 62 ($M_m \geq 5.0$) mainshocks (1933–1987) in California. They used aftershocks with the magnitude $M_a \geq M_m - 3.0$. For these sequences they obtained an average value of the c coefficient of 0.05 days. Figures 4, 5, 8, and 9 and equations (18) and (19) in general confirm their result.

Size Distributions

Figure 10 displays the normalized magnitude–frequency relations for short-term aftershocks of the 1992 Landers earthquake. Aftershocks are sampled in logarithmically increasing time intervals. Aftershocks in the early part of the sequence are clearly depleted of smaller events. For comparison I also show earthquake size distribution for the same spatial window in the period 1990–2001. The magnitude–frequency plot for larger aftershocks is approximately parallel to the 1990–2001 curve, but for smaller earthquakes there is a deficit of events. Only for the largest time intervals (more than 8 days) are the aftershock curves parallel to the 1990–2001 curve over the entire magnitude range.

The magnitude–time plot in Figure 5 confirms this pattern: even its visual inspection suggests that many weak earthquakes are missing or underreported from the catalog in the first hours and days of the aftershock sequence. The display for the Landers earthquake (not shown), similar to Figure 7 and Figure 9, also supports this observation.

Wiemer and Katsumata (1999, their figure 2) have shown that the magnitude threshold M_t for the Landers aftershocks rises significantly in the immediate wake of the mainshock. They obtained the values $M_t = 2.9$ and 2.7 for the time interval closest to the mainshock origin time and

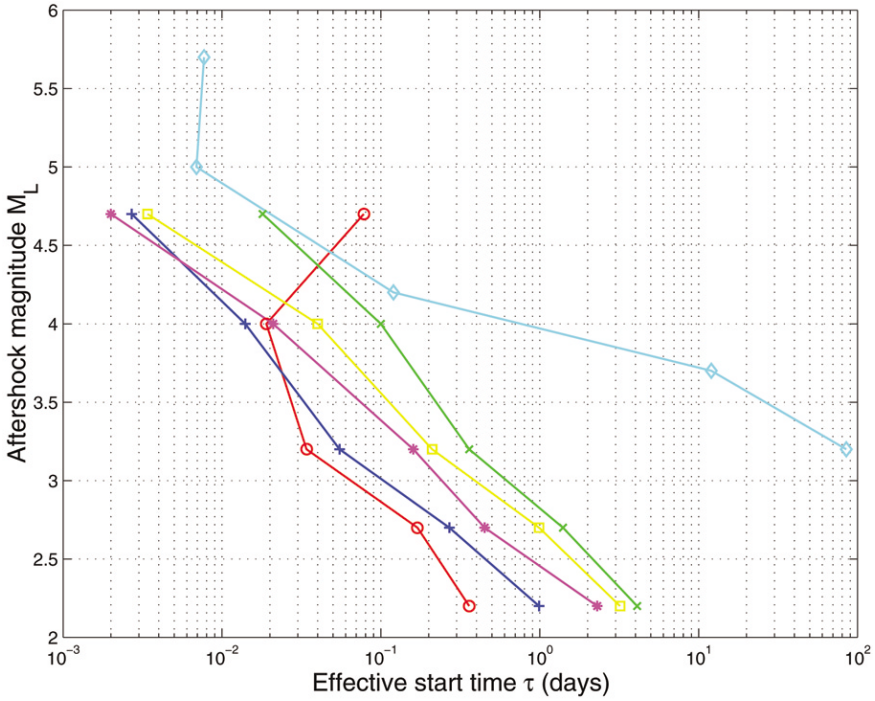

Figure 9. Effective starting time τ_0 for aftershocks of southern California earthquakes. Diamonds, 1952 $M = 7.5$ Kern County; circles, 1992 $M = 6.1$ Joshua Tree; crosses, 1992 $M = 7.3$ Landers; squares, 1992 $M = 6.5$ Big Bear; pluses, 1994 $M = 6.7$ Northridge; stars, 1999 $M = 7.1$ Hector Mine.

for the northern and southern Landers aftershock zone, respectively. This is significantly smaller than one would obtain from the first two closest curves in Figure 10 by simply extrapolating curves to the ordinate equal to 1.0. What is the most likely reason for such a discrepancy? Wiemer and Katsumata (1999) used 300 events to obtain the M_t value. As Figure 5 demonstrates, the magnitude threshold decreases rapidly with the increase in time interval; thus, if one averages the magnitude–frequency relation over many aftershocks, this would yield only the average M_t value, which may misrepresent the high-magnitude threshold value for short-term aftershocks.

Wiemer *et al.* (2002, their figure 2) repeated similar determinations of M_t for the Hector Mine aftershock sequence. They obtained as the highest M_t value about 3.5; the threshold magnitude reached the value 2.0 after only 3 days. They used 100 events for determining the M_t. Due to the smaller event number, these results may better agree with Figure 8, where we see $\tau_0 \approx 3$ days for M 2 and $\tau_0 \approx 0.01$ days for M 4.

In Figure 11 I summarize the results of the b-value determination in logarithmic time intervals for five aftershock sequences. I evaluate the b-values using equation (15) and use $M_t = 2$ for all sequences except the Kern County earthquake, for which $M_t = 3$ is applied. For small time intervals the b-values are strongly biased due to the lack of small aftershocks in the catalog. However, by comparing these values to the b-value for the whole southern California area (solid line, $b = 1.0$), I again infer the properties of short-term aftershocks. The b-values reach the 1.0 level at time intervals approximately equal to τ_0, when the time-dependent threshold magnitude reaches the level of the general M_t for southern California (Fig. 9).

The b-values continue rising slowly even for larger time intervals. This pattern, increasing b-values in the later part of the aftershock sequences, is found in many investigations. However, it has been obtained through a retrospective analysis of earthquake catalogs. During such an analysis, earthquake sequences are subdivided into foreshocks, mainshocks, and aftershocks, a categorization possible only after the whole sequence of events is available. Frohlich and Davis (1993) found that the difference in b-values for mainshocks and aftershocks is caused by some subtle systematic effects due to event selection. In real-time evaluation, one does not know whether a large earthquake will be followed by an even larger event. Therefore, predicting a lower b-value in the wake of such an earthquake would depend on the condition that this earthquake is not a foreshock of a stronger event.

Missing Earthquakes

As discussed earlier, many short-term aftershocks are missing (or underreported) from the catalog. How can I at least approximately evaluate their number? I first need to define missing events. One way to define missing earthquakes is a comparison of different earthquake catalogs.

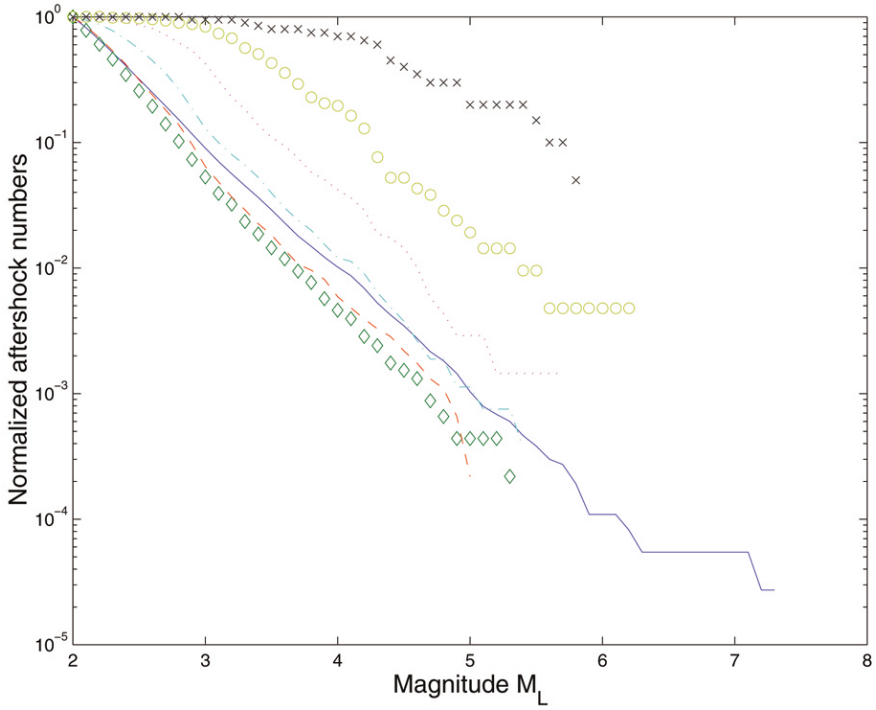

Figure 10. Magnitude–frequency distribution for 1992 M 7.3 Landers, California, aftershocks. The window of latitude 33.5°–36.0° N, longitude 116.0°–118.0° W is used; time interval is 128 days after the mainshock. Solid line, all earthquakes in 1990–2001, $n = 36{,}643$; crosses, aftershocks less than 0.063 days, $n = 20$; circles, aftershocks 0.063–0.5 days, $n = 209$; dotted line, aftershocks 0.5–2 days, $n = 690$; dash-dotted line, aftershocks 2–8 days, $n = 2655$; dashed line, aftershocks 8–32 days, $n = 4570$; diamonds, aftershocks 32–128 days, $n = 4559$.

Kagan (1991a, 2003) discussed many cases where earthquakes listed in one catalog are not shown in another data set, even if the reported magnitude is well above the magnitude threshold of the latter catalog (see also Fig. 6). Usually such a difference is observed for clustered events, as in aftershock sequences. Local catalogs normally report more events than global data sets. The number of such underreported events in global data sets is usually a few percent of the total earthquake number.

However, here I am interested in missing short-term aftershocks due to overlapping records and other effects; inspecting Figures 4, 5, and 7–9 suggests that their number may be significant. Earthquake catalogs are constructed by determining location, magnitude, origin time, and sometimes the parameters of earthquake focal mechanism through interpretation of seismograms. The most important factor here is earthquake location; if it has not been determined, it is usually impossible to estimate other characteristics. The location (hypocenter coordinates) is generally determined based on the arrival time of body waves. Such arrivals are difficult to find if seismic records overlap when several earthquakes have occurred in approximately the same time and location. This commonly happens at the beginning of an aftershock sequence.

However, the effects of such overlapping can be alleviated by using higher-frequency seismograms from stations closer to the earthquake source region. For example, Vidale *et al.* (2003) found "several times more events in the first few minutes than are recorded in the best catalogs" in high-pass filtered seismograms.

Even in local catalogs there is a significant time gap between the end of the mainshock rupture (t_r in equation 17) and the beginning of the aftershock sequence (see Figs. 4–6). If a very strong aftershock comparable in magnitude to a mainshock were to occur near the rupture end, it might be attributed to the mainshock process as a late subevent, extending the rupture duration. Hence, depending on the time delay and the seismologist's decision, a very large aftershock may appear early at any place in an aftershock sequence. Moreover, a gap in the short-term aftershock sequence could be a factor in identifying the main phase of earthquake rupture. Thus, one cannot base the definition of the beginning time on an observation of only a few events.

As soon as the beginning of an aftershock sequence is selected, the number of missing earthquakes can be computed easily. I extrapolate the temporal aftershock distribution to the starting time as shown, for example, in Figure 3. In Figure 12 I display the results of this extrapolation for the 1992 Landers aftershocks. The extrapolation goes to either the t_r value (equation 17) or to the $32 \times t_r$ value, which

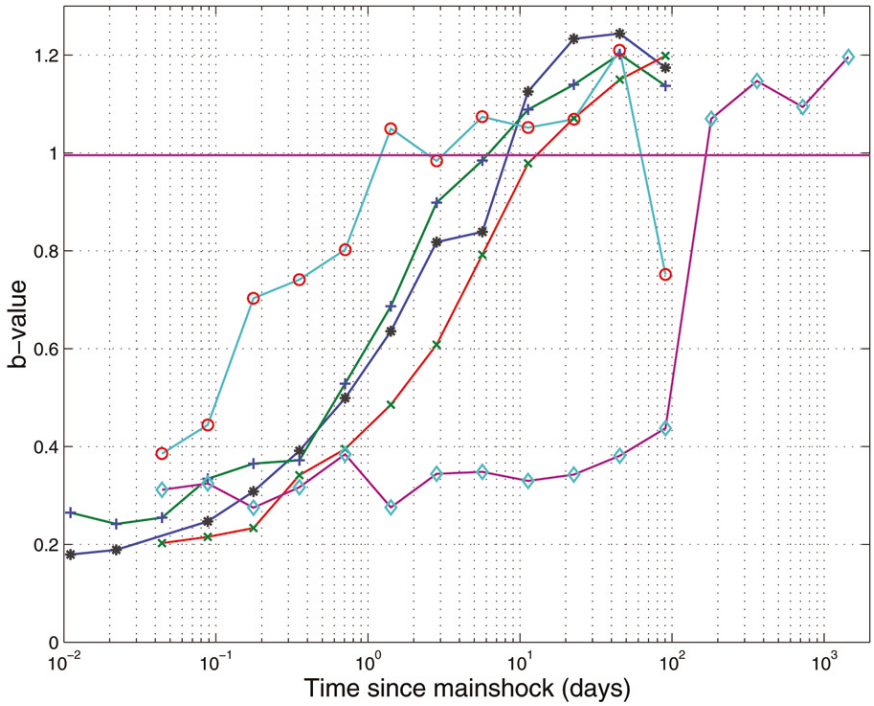

Figure 11. Temporal behavior of *b*-values for aftershocks of southern California earthquakes. Solid line, *b*-value for 1990–2001 seismicity in the window latitude: 32.5°–36.0° N; longitude: 115.0°–121.0° W; $n = 50{,}664$; diamonds, 1952 M 7.5 Kern County; crosses, 1992 M 7.3 Landers; stars, 1994 M 7.1 Hector Mine; pluses, 1994 M 6.7 Northridge; circles, 1992 M 6.1 Joshua Tree.

corresponds roughly to observing the first strong aftershocks, or to the t_M value (equation 18).

For the first extrapolation curve, the number of small ($M \leq 3.0$) missing aftershocks exceeds the number of registered events. For the smallest events (M 2), the ratio of underreported to registered aftershocks is about 3. The total number of missing events is about 28,000, that is, it exceeds the total number of aftershocks in the time interval of 0–128 days by a factor of 2.2 and is comparable to the total number of earthquakes in southern California in the 1990–2001 period ($n = 50{,}664$; see Fig. 11). The situation is similar for the second curve. Increasing the beginning time of an aftershock sequence by a factor of 32 does not significantly change the events ratio: the total for missing aftershocks is about 17,500. The number of underreported events significantly differs for the third curve, where I extend the beginning time of aftershock sequences toward the t_M value (equation 18). The total number is 9001, and almost all (8924) are in the magnitude interval $3.0 > M \geq 2$. Only these numbers are comparable to the numbers of registered aftershocks. As mentioned earlier (near equation 18), this t_M value has been selected for catalogs with a more limited magnitude range than the present CIT catalog.

In all of these calculations I counted the primary aftershocks only (i.e., those that are due to the mainshock). Each of these strong aftershocks may have its own subsequence of secondary aftershocks. In the secondary sequence, short-term events may not be registered either (see the τ values for the Big Bear aftershock in Fig. 9). The total effect of this clustering is a lack of additional earthquakes. Therefore, the number of missing earthquakes shown is considered conservative.

Global Seismicity

I analyze two global earthquake catalogs: the PDE and the Harvard lists. Instead of considering a few strong earthquakes as in the CIT catalog, this investigation takes all shallow (0–70 km) earthquakes greater than M 6 as mainshocks and looks for an earthquake pattern following these events. Some of these strong earthquakes can be foreshocks or aftershocks of preceding events. In principle, one could set up window boundaries conditional to the occurrence of strong earthquakes in the neighborhood of the aftershock sequence to be investigated. However, these conditions may become complicated and the results of the analysis turn out less transparent and reproducible. Since I am interested in short-term aftershock sequences, the effects of the sequence overlap would be small. To faithfully take into account the clustering effects of strong earthquakes, one would need to apply the methods of stochastic point processes (Kagan and Knopoff, 1987b; Ogata, 1988, 1998; Kagan, 1991b). Again, in this preliminary study I want to use the simplest methods, so that results can easily be understood.

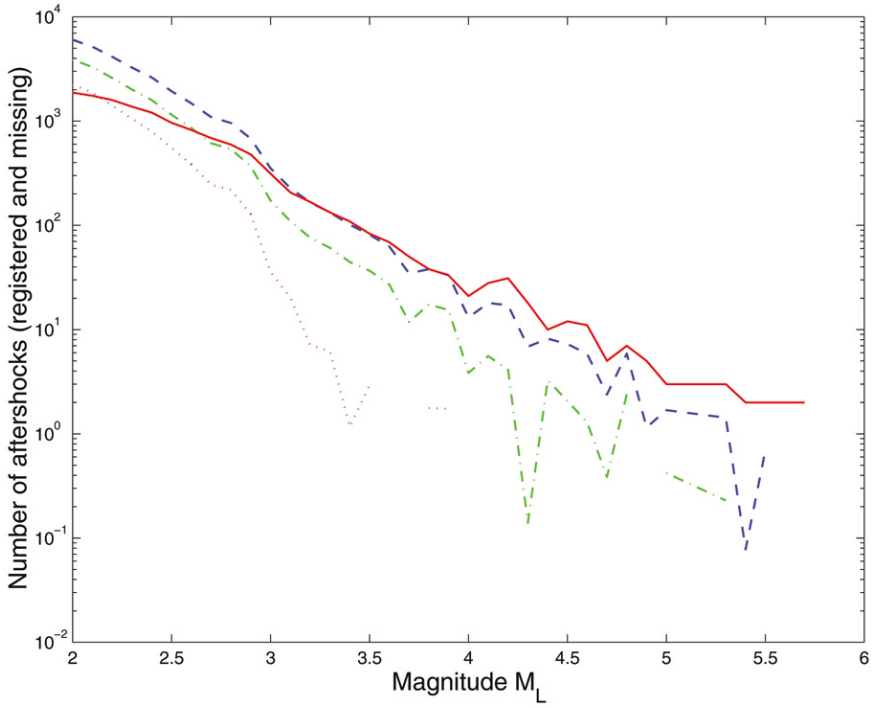

Figure 12. Comparison registered and missing aftershocks of the 1992 M 7.3 Landers, California, earthquake. Solid line, registered events; dashed line, missed events, extrapolation to t_r, see equation (17); dash-dotted line, missed events, extrapolation to t = 32 t_r; dotted line, missed events, extrapolation to t_M, see equation 18.

Since the magnitudes in the PDE catalog (m_b and M_S) saturate for large magnitudes (Kagan, 1991a, 2003), in analyzing aftershock patterns in this catalog I use mainshocks from the Harvard catalog. I determine moment magnitude in the CMT list by the formula

$$M_w = \frac{2}{3} \log_{10} M_0 - 6.0, \qquad (20)$$

where scalar seismic moment M_0 is measured in newton meters.

Kagan (2003) determined magnitude thresholds for the Harvard catalog. These thresholds are lower than 6.0 throughout the 1977–2001 catalog. Therefore, all CMT mainshocks are complete. However, to study aftershock sequences for the CMT list (discussed later) I select the 1982–2001 subcatalog with the threshold M_t 5.6.

The magnitude threshold for the PDE catalog is more difficult to evaluate. Several magnitudes are listed in the catalog; their threshold changes over time and seismic regions. Kagan and Knopoff (1980) found the PDE threshold around 5.0 and selected M_t 5.3 in their seismicity analysis. Habermann *et al.* (1993) determined the m_b magnitude threshold around 5.0 for the PDE catalog. Willemann (1999a,b) showed that the m_b threshold changes in time and space for the ISC catalog and suggested that the M_t values fluctuate between 4.0 and 5.0. The PDE thresholds should be similar to those of the ISC catalog. I decided to use M_t 4.5 for the PDE catalog here; this value is most likely too low an estimate, but would yield a greater number of aftershocks that can be used to evaluate the basic properties of short-term sequences.

In selecting shallow (0–70 km) aftershock sequences in global catalogs, I use the time limit of 128 days and a spatial circular window with a radius, R:

$$R = 20 \times 10^{(M-6)/2} \text{ km}. \qquad (21)$$

The radius is larger by a factor of 2 than the one used in equation (16), since location errors are higher in global catalogs (Kagan, 2003).

Figure 13 displays the numbers of aftershocks in the PDE global catalog in a format similar to Figure 7. Contrary to the plots in the California earthquakes section, we use combined (stacked) aftershock sequences of many mainshocks here. Some very large mainshocks may have only a few aftershocks, whereas others have extended aftershock sequences. All the curves show similar behavior. The number of aftershocks is approximately uniform at larger logarithmic time intervals, indicating that generally aftershocks follow the simple Omori law (equation 3). For smaller time intervals, the aftershock rate decays and the decay rate is stronger for smaller aftershocks.

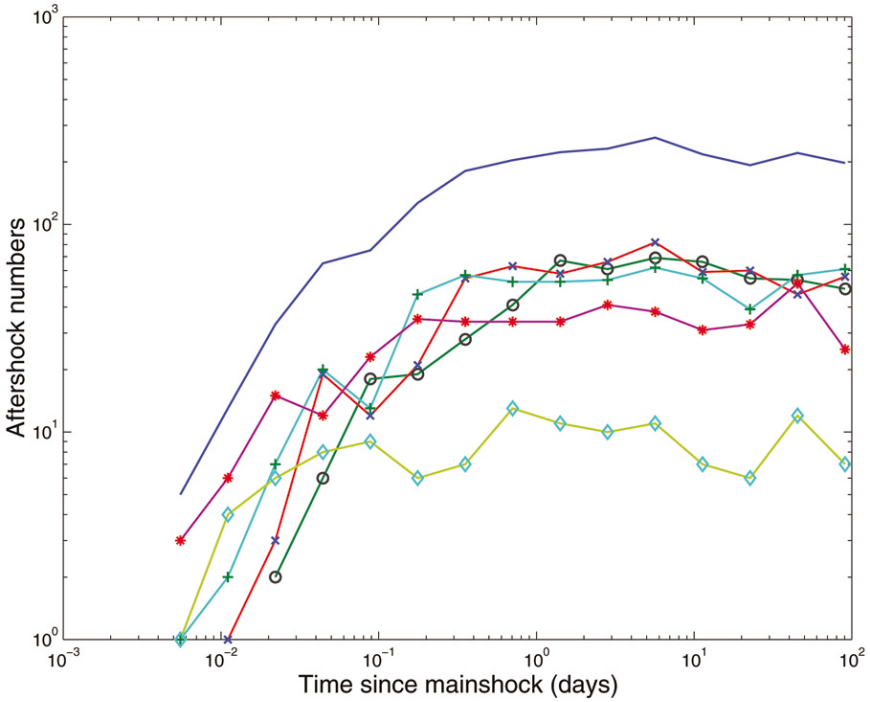

Figure 13. Aftershock numbers for the PDE global earthquake catalog; time limits are 1 January 1977 to 31 December 2001. Time interval limit is 128 days after the mainshock. Solid line, all aftershocks; circles, aftershocks $4.6 \geq m_b \geq 4.5$; crosses, aftershocks $4.8 \geq m_b \geq 4.7$; pluses, aftershocks $5.1 \geq m_b \geq 4.9$; stars, aftershocks $5.7 \geq m_b \geq 5.2$; diamonds, aftershocks $m_b > 5.7$. Magnitude limits for mainshocks are $M_w \geq 8.0$, the mainshock number is 14, and the aftershock numbers are 2250, 535, 601, 580, 416, and 118, respectively.

Figure 14 shows the τ_0 curves for mainshocks of different magnitude ranges. The m_b aftershock sequences begin earlier than the M_S aftershocks. The former magnitude is determined by the 1-sec *P* waves, whereas the M_S magnitude is based on the 20-sec surface waves, which are more difficult to identify in the mainshock coda. Although stronger mainshocks generally have a longer delay in their aftershock sequences, the τ_0 dependence on M_m is not as obvious as in Figure 9. It is difficult to understand what causes such a difference. It may be due to interference of several aftershock sequences in complex earthquake clusters (see the beginning of this section), but additional investigations are needed.

Figure 15 shows the numbers of registered and missing aftershocks for $6.5 > M \geq 6.0$ CMT mainshocks, using the m_b magnitude in the PDE catalog. From the behavior of the magnitude–frequency relation closer to the magnitude threshold, one sees that the M_t value needs to be higher to ensure the completeness of the catalog; M_t 5.0 seems to be a more appropriate choice. The number of missing aftershocks for the t_r starting time is high, comparable to the number of registered events.

The numbers of missing events remain relatively high if I increase the beginning time for aftershock sequences to $64 \times t_r$, that is, the time when the first aftershocks appear in the PDE catalog (cf. table 3 in Kagan [2003]). From Figure 6 and similar observations of aftershock sequences in local and global catalogs, the starting time for m_b aftershocks should be greater than the time for the local catalogs. The missing event numbers for M_t 4.5 are about 300–700 for each of the mainshock magnitude intervals. If the magnitude threshold is raised to M_t 5, the numbers are around 30–150. This means that the PDE catalog is significantly nonuniform in the wake of strong earthquakes. However, if one excludes all aftershocks closer than t_M from the catalog, there are a few missing aftershocks. There are a few underreported events in the mainshock magnitude range $6.5 > M \geq 6.0$ only. These events may be due to overlapping aftershock sequences in complex records of strong earthquakes.

A similar study of the CMT catalog shows that the number of missing earthquakes is relatively small. Since the CMT catalog is based on an analysis of low-frequency waves, the first aftershocks are registered later than in the PDE or CIT catalogs. Figure 6 in Kagan (2003) suggests that the aftershock starting time is about 0.06 days for earthquakes in this $8.0 > M \geq 7.5$ magnitude range. Calculating the number of missing aftershocks using $t_r \times 256$ starting time yields values smaller by an order of magnitude compared to the number of registered events. If one increases the beginning time to t_M (equation 18), the number of missing events becomes so small that we can neglect this effect in most statistical analysis problems.

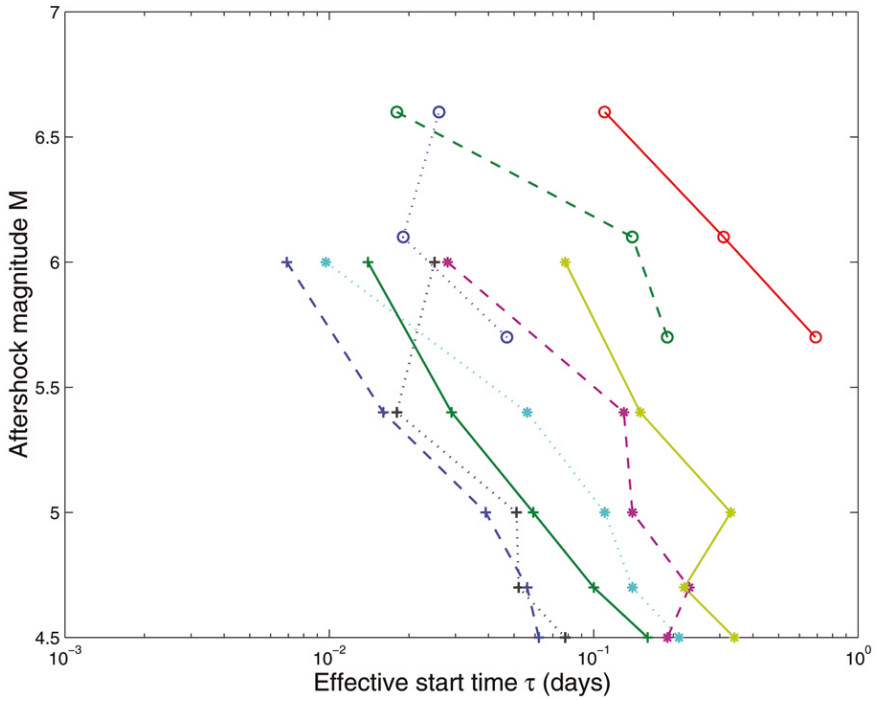

Figure 14. Effective starting time τ for aftershocks of the two global catalogs (PDE and CMT). Magnitude limits; dotted line, $6.5 > M_w \geq 6.0$; dashed line, $7.5 > M_w \geq 7.0$; solid line, $M_w \geq 8.0$. The respective mainshock numbers are 1478, 124, and 11 for the CMT catalog and 1822, 166, and 14 for the PDE list. Circles, CMT aftershocks; stars, PDE aftershocks, M_S magnitude; pluses, PDE aftershocks, m_b magnitude.

Representing Earthquake Sources

What do the results of the previous sections signify for models of earthquake source? From what I see in the short-term distributions of aftershock numbers, it appears likely that the c coefficient in the Omori law representations (equations 1–3) is close to zero. A partial confirmation for such a conclusion can be found in many observational attempts to estimate the value of the coefficient and to determine its relationship to tectonic and geophysical variables. Empirical c values exhibit great, seemingly unpredictable variations (Utsu, 1961, 1969; Ogata, 1983, 1998; Davis and Frohlich, 1991; Utsu *et al.*, 1995; Nyffenegger and Frohlich, 2000). However, from table 1 in Utsu *et al.* (1995) or tables 2–5 in Narteau *et al.* (2002), it is clear that for stronger aftershocks $c \to 0$.

The condition $c = 0$ implies a singularity: infinite energy release at the earthquake origin time. However, the Omori law (equations 1, 2) is formulated for an instantaneous model of earthquake source. Clearly, it should be modified as soon as earthquake rupture over an extended source region is considered. One possibility of such modification is to use the c coefficient comparable in value with earthquake rupture time, t_r. But such a model would not predict decay of the aftershock rate for times very close to the mainshock time, when no aftershocks are registered during the rupture process. Secondly, it would fail to connect aftershock occurrence with the complexity of earthquake rupture.

Is this relative lack of short-term aftershocks due to the properties of earthquake source, or can it be partly attributed to various technological and administrative factors? If the latter assumption is true, then the behavior of long-term aftershocks can be extrapolated to very short time intervals and, finally, to the earthquake rupture process itself. Recent results for inversion of earthquake rupture history, using seismological, geological, and geodetic data (see subsequent text and the Introduction), strongly suggest that over very short time intervals rupture propagates as a slip pulse (Heaton, 1990). The pulse exhibits great variations in amplitude, propagation velocity, direction of displacement, and geometric complexity of fault zone. Do these arguments mean that rupture propagation complexity can be represented by a mechanism similar to aftershock occurrence? To answer this question we need to consider various representations of earthquake source.

Observational Evidence

In the least detailed representation, the source is given as a point in a multidimensional space, that is, as a delta function:

$$\delta\ (t,\ \mathbf{x},\ M,\ \mathbf{q}), \tag{22}$$

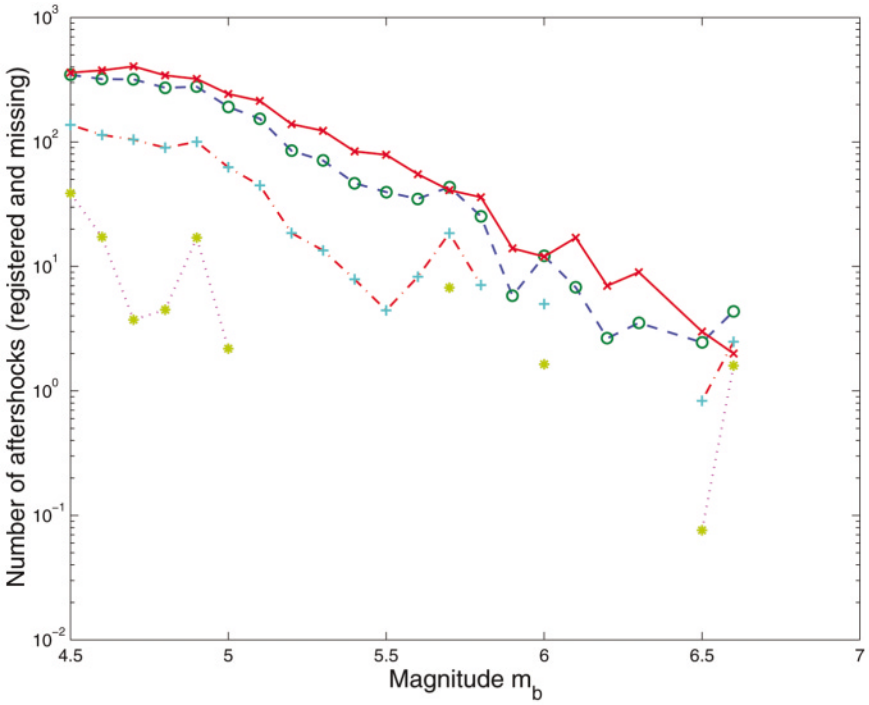

Figure 15. Comparison registered and missing aftershocks in the PDE catalog (m_b magnitude) for $6.5 > M \geq 6.0$ CMT mainshocks. The mainshock number is 1822. Solid line, registered events; dashed line, missed events, extrapolation to t_r, see equation (17); dash-dotted line, missed events, extrapolation to $t = 64\ t_r$; dotted line, missed events, extrapolation to t_M, see equation (18). If intervening values are zero, signs are not connected by a line.

where x are the coordinates of a hypocenter and q is a normalized quaternion, a short description of a double-couple focal mechanism (Kagan, 1982). The models, using stochastic point processes (Kagan and Knopoff, 1987b; Ogata, 1988), assume this representation of the earthquake process.

The next step in a more detailed representation of the earthquake process involves describing earthquakes as sources extended in time and space with varying focal mechanisms. Commonly such descriptions are available only for particular earthquakes or sets of a few earthquakes. Recently new catalogs started to appear in which the earthquake process develops in time (Tanioka and Ruff, 1997; see www.geo.lsa.umich.edu/SeismoObs/STF.html) or as seismic moment rate release in space-time (McGuire *et al.*, 2001). In a series of papers, Houston (2001, and references therein) analyzed temporal behavior of seismic moment release. Earthquake time functions displayed in her figure 6 show a complex release of seismic moment, in many cases several separate subevents can be identified.

In the final detailing of extended sources, the earthquake rupture process is presented in the issues of the *BSSA* mentioned earlier. These article collections describe earthquake rupture history as a slip over an assumed fault plane or fault planes propagating with near elastic wave velocity. Several time-space history maps for mainshocks were published in the *BSSA:* for Loma Prieta, Wald *et al.* (1991); for Landers, Cohee and Beroza (1994), Wald and Heaton (1994); for Northridge, Wald *et al.* (1996), Zeng and Anderson (1996), and Thio and Kanamori (1996); Chi-Chi, Chi *et al.* (2001), Ma *et al.* (2001); Izmit, Delouis *et al.* (2002), Bouchon *et al.* (2002); and Hector Mine, Kaverina *et al.* (2002). In these articles, rupture velocity is found within 50%–85% of the *S*-wave velocity, although in one case (Bouchon *et al.* [2002]) a super-shear velocity is suggested. The velocity is often not constant, and time delays in rupture propagation are also indicated. The slip distributions are very complex; in some cases (Delouis *et al.* [2002], Kaverina *et al.* [2002]), slip events behind main slip pulse are noticed. The geometry of the fault zone as revealed by Earth surface ruptures is complex; often fault branching is also seen.

Deterministic and Stochastic Models of Earthquake Source

In all deterministic representations of earthquake source (Aki and Richards, 1980), the rupture process is modeled as a combination of delta functions with smooth distributions of slip over time and space subsets. For example, earthquake slip onset is usually represented as a ramp function, which can be expressed as

$$\iint [\delta(t_1 - x/v_x) - \delta(t_2 - x/v_x)]\, dt^2, \qquad (23)$$

where $t_2 - t_1$ is the rise time of a rupture pulse and v_x is the propagation velocity in the x direction.

Thus, the standard models of earthquake occurrence envision strong delta function singularities in time and space. These models fail to explain the temporal complexity of earthquake rupture and aftershock occurrence or the geometric complexity of the earthquake fault system. Additional assumptions and hypotheses are commonly invoked to explain earthquake source complexity.

Since the late 1980s many models of the earthquake process employing scale-invariant or fractal formalism have been proposed, some based on a concept of the self-organized criticality (for example, Bak and Tang [1989] and Cowie *et al.* [1995]; for more extended reviews see Main [1996] and Sornette [2000]). However, all these models envision an earthquake (mainshock or aftershock) as an individual event. Hence the complexity of earthquake sources needs to be explained by a separate mechanism.

Frankel (1991) and Zeng and Anderson (1996) proposed representing an earthquake as a large collection of subevents with a fractal distribution of their sizes. Earthquake propagation is seen as rupture jumping from one subevent to another.

In a fractal model of earthquake rupture propagation (Kagan and Knopoff, 1981; Kagan, 1982), we proposed considering each subevent (Frankel, 1991) as a tight cluster of elementary dislocations. The fractal model replaces delta function singularities in time, space, and focal mechanism by weaker power-law singularities. For instance, the delta function in time (or an integral of a delta function, see equation 23) is replaced by the Omori law–like distribution (pdf) of time delays (Δt) between elementary subevents:

$$\phi(\Delta t) \propto (\Delta t)^{-1-\theta}, \qquad (24)$$

where the exponent θ is close to 0.5 for shallow seismicity (Kagan and Knopoff, 1981).

Similarly, the spatial characteristics of earthquake rupture are usually represented as a delta function. Let us use the coordinate system $\mathbf{x} = \{x, y, z\}$, so that the x and y coordinates are in a fault plane. Then $\delta(z)$ represents the fault plane in the standard (Euclidian) models of earthquake rupture (Ben-Zion and Sammis, 2002). Kagan (1982) proposed to replace the delta function by a weaker singularity:

$$\phi(z) \propto \frac{1}{z}. \qquad (25)$$

A comparable distribution controls variation of focal mechanism orientation: almost all 3D rotations of the focal mechanism are very small, although occasionally a fault plane is allowed to branch or a slip vector to change its direction significantly (Kagan, 1982). The variation of earthquake slip amplitude is also controlled by a fractal branching mechanism. The weaker singularities, as shown in equations (24) and (25), can be incorporated naturally in a stochastic model of earthquake rupture development, replicating complex features of earthquake occurrence.

Simulations based on the fractal model of earthquakes reproduce visual characteristics of earthquake fault systems and the temporal complexity of earthquake moment release during earthquake rupture and foreshock/aftershock sequences (Kagan and Knopoff, 1981; Kagan, 1982). The statistical properties of synthetic sequences are also similar to those obtained in empirical analysis.

Thus, the fractal model envisions both the short- and long-term rupture process as discontinuous everywhere in time-space-focal mechanism manifold. However, almost all the jumps are infinitesimal, that is, well below the resolution power of observation systems. Therefore, nearly continuous tight clusters of subevents are interpreted as individual earthquakes—foreshocks, mainshocks, and aftershocks—while the degree of such subdivision depends on the available resolution technology.

The consequences of the fractal model are substantial. For example, I compute the number of elementary subevents necessary to model the seismicity of southern California. Field *et al.* (1999) proposed that the total seismic moment rate is approximately 10^{19} N m/yr. If one would like to represent earthquake occurrence at the level M 2 shocks, on average 10^7 events/yr would be necessary. Surely, as mentioned earlier, these subevents would be concentrated in groups with little variation of the basic parameters: these subsets would normally be recognized as individual earthquakes. However, with increased resolving power of modern instrumentation and computing capability, such a fractal representation may become normal in future earthquake occurrence analysis.

Investigating Short-Term Seismicity Patterns

What are the possibilities for observationally confirming the fractal model of earthquakes and in particular the behavior of short-term aftershocks in the time period between the end of the mainshock rupture and the emerging power-law temporal decay for weaker aftershocks? Presently determining earthquake parameters is based both on the arrival times of earthquake body waves and constructing a hypocenter solution using these times. More sophisticated methods of body-wave correlation (see, for example, Waldhauser and Ellsworth [2000]) have significantly improved hypocenter location accuracy, but these methods cannot resolve overlapping, complex seismic records in short-term aftershock sequences. Perhaps a systematic effort to interpret these seismograms using traditional methods may yield a significant number of additional earthquake events (Vidale *et al.*, 2003).

Placing many seismographic stations in an earthquake focal zone and boreholes should also help to identify close-in-time aftershocks. However, when one approaches the mainshock closer in time, the traditional methods of seis-

mogram interpretation would eventually fail, since strong coda waves of a mainshock and strong aftershocks immediately following it make identifying body-wave arrivals impossible.

Presently coda waves are modeled as randomly scattering waves in a laterally heterogeneous medium (Sato and Fehler, 1998). To obtain the entire history of earthquake occurrence, one would need to deconvolve overlapping seismic records immediately following a large earthquake. To accomplish this, one should model the entire wave train of an earthquake, that is, to faithfully reproduce the Green's function for an earthquake. Increased computer power may enable this approach by using either an empirical Green's function of later aftershocks for deconvolution or by computing the 3D theoretical synthetic Green's function for a laterally inhomogeneous Earth (Bunge and Tromp, 2003).

Discussion

Properties of short-term aftershocks have not been the focus of seismological research. Therefore, no special effort was spent in properly arranging the seismographic network, collecting specific data, and analyzing the results. The available short-term catalog data apparently have drawbacks similar to data on earthquakes below the magnitude completeness threshold: although catalog compilers commonly include these events in a data set, apparently less attention is paid to ensure the uniformity of time and space coverage. Here I consider the problems specified in the Introduction.

Statistical Analysis of Earthquake Catalogs

In the statistical analysis of earthquake catalogs, it is important to have a catalog uniform in time, space, and magnitude. Catalog nonuniformity may introduce unexpected biases into the results of statistical analysis. For example, I show that the magnitude distribution for the short-term aftershocks significantly differs from the distribution of all other events and long-term aftershocks. This size distribution difference is caused mainly by missing small aftershocks, that is, it is most likely an artifact.

There is another significant consequence of this study for many interpretations of statistical properties of seismicity. As suggested in the previous section, identifying an *individual* earthquake cannot be justified objectively. What is usually considered an earthquake event is not a well-defined physical entity, but the result of a complex process of registration and interpretation where properties of seismographic network and seismogram processing techniques determine, to a crucial degree, what would be called *an* earthquake. For example, figures 2 and 3 in Houston (2001) demonstrate that earthquake source time functions determined by various investigators may differ significantly, in her figure 15 earthquake durations measured by Tanioka and Ruff (1997) and Bilek and Lay (1999) often disagreed by a factor of 2 and more. Figure 6 and many examples in Kagan (2003) demonstrate that in different earthquake catalogs the same sequences are represented by different numbers of earthquakes.

Kagan (1991a) argued that an earthquake *sequence* may be better suited for analysis as an independent entity. The total seismic moment of a sequence does not depend on how many individual earthquakes the sequence is subdivided into. Commonly used earthquake catalog declustering (removing aftershocks) attempts a similar job, since mainshocks remaining in a declustered catalog are, in principle, statistically independent. Hence, they can be considered as individual entities. Declustering is difficult because (1) an aftershock cannot be unambiguously identified and (2) deleting these events leaves holes in a catalog that may again lead to biases.

The CMT catalog, which uses long-period seismic records and includes many short-term aftershocks in its definition of a mainshock (Kagan, 2003), comes closer to a set of earthquake sequences than other data sets. This is one reason that the earthquake size distribution results obtained from this catalog are more robust (Kagan, 1991a).

The process of earthquake catalog compiling is not currently formalized or even well described. Hence, only by careful catalog inspection can one infer properties and biases. This lack of sufficient knowledge for the seismogram–catalog transition hampers any attempt to model the earthquake process for comparing the model predictions to empirical data. Therefore, in interpreting the results of statistical analysis of catalogs, one must be aware of which perceived regularities are due to catalog compilation peculiarities and which (if any) to physical processes of earthquake occurrence. Moreover, in analyzing seismicity patterns statistically, a clear distinction should be made between empirical seismicity models (like Kagan and Knopoff, 1987b; Ogata, 1988; Kagan, 1991b; Kagan and Jackson, 2000) that may be appropriate for earthquake potential forecast purposes and stochastic models that attempt to reproduce underlying physical process (Kagan and Knopoff, 1981; Kagan, 1982).

Theoretical Modeling of Earthquake Occurrence

This work has implications for theoretical models of earthquake occurrence and rupture. First, from statistical analysis of short-term aftershocks, it seems likely that the c coefficient in the Omori law formulation (equations 1–3) is not a physical property of an earthquake process, but reflects various instrumental and man-made factors. The real value of the coefficient is more likely close to the rupture time of an earthquake, that is, the time when the point model of earthquake source is no longer valid. If this conjecture is true, then the c value depends on geometrical and kinematic properties of the earthquake source zone. This would imply that the models employing a nonzero c coefficient need to be revised.

The second and more important conclusion of these investigations relates to the problem of earthquake identification. If the earthquake process is controlled by a fractal distribution, then designating an individual earthquake again

depends on technological and subjective features, as described in the previous subsection. Thus, an earthquake does not represent a well-defined physical object. In almost all physical models of earthquake occurrence, defining an earthquake or an earthquake fault is crucial to model functioning.

Although the beginning of a shallow earthquake rupture is commonly (but not always) quite abrupt, its end is difficult to define unambiguously. Aftershocks immediately follow the mainshock rupture, and existing technology does not allow us to identify short-term aftershocks reliably. When such identification becomes possible, where and how does one draw a boundary between the end of one earthquake rupture and a quiet period preceding the next earthquake occurrence? Considering the possibility that the G–R relation can be extended to magnitude values well below zero, and since an earthquake rupture at a lower level may be continuing during the aftershock sequence, does the quiet-period exist at all? An earthquake identification may depend on a numerical value for the quiet-period criterion. Hence, different criteria would yield various earthquake numbers.

A Fractal Model of Earthquake Source Process

The results of this study make the fractal model of earthquake process proposed by Kagan and Knopoff (1981) and Kagan (1982) more convincing. Until recently the resolution power of seismic and geodetic instruments and computing power were insufficient to retrieve necessary details of the earthquake rupture process. In the near future it may be possible to obtain both a detailed rupture history of earthquakes and a progression of dependent subevents (fore- and aftershocks) as an indivisible picture of the rupture process.

Kagan and Knopoff (1987a) and Kagan (1990), (see also Zolotarev [1986]; Uchaikin and Zolotarev [1999]) proposed that the temporal and spatial complexity of the earthquake source is due to random defects that yield fractal distributions of static stress in a rock medium. The short-term earthquake processes considered in this article have a kinematic character. Hence, the dynamic stress (see, for example, Gomberg *et al.* [2003]) of earthquake rupture should play a major role in earthquake subevents and close-in-time aftershocks. In reality the difference between the static and dynamic stress approach may not be as great, since the defects mentioned previously may correspond to small earthquakes below an observational threshold. These infinitesimal earthquakes occur constantly in the stressed Earth interior. As a consequence, the dynamic stress of these shocks could produce a seemingly random earthquake occurrence.

In the regions of low tectonic deformation, the Omori law is observed for time periods of hundreds of years (Utsu *et al.*, 1995; Ebel *et al.*, 2000). It seems likely that earthquake rupture is a complex phenomenon that can be considered a model of the fundamental features of the entire earthquake process, including its long-term properties. In the final short-term extrapolation, the Omori law seems more fundamental than the G–R relation. The latter depends on identifying individual earthquakes, which, as we have seen, cannot be defined unambiguously at short-term intervals. By contrast, the Omori law is valid even for elementary dislocations that constitute an earthquake source.

Conclusions

1. Short-term aftershocks are significantly incomplete in both local and global earthquake catalogs. The incompleteness is more severe for small aftershock events, although even strong aftershocks may be absent closer to the mainshock rupture end. The reasons for this incompleteness are diverse: limitations of the seismographic network, overload of processing facilities in the beginning of aftershock sequences of strong mainshocks, and fundamental difficulties in interpreting complex overlapping seismic records.
2. The number of missing earthquakes in extensive aftershock sequences depends on the magnitude range of a catalog and the seismogram frequency range. For local earthquake catalogs, like the CIT, such a number may be comparable or even exceed the total number of earthquakes in a catalog. Analyzing worldwide earthquake catalogs shows that a significant number of smaller aftershocks are not recorded in the PDE catalog. For the CMT catalog only with its relatively small magnitude range (5.5–8.5) and use of low-frequency recording, the number of underreported events is insignificant.
3. These deficiencies in earthquake catalogs, unless fully explored, may introduce substantial biases in the results of statistical analysis.
4. The large nonzero values for the c-coefficient in the Omori law are most likely due to missing aftershocks, especially small ones. Closer to the mainshock origin time, the point model of earthquake source breaks down. Hence, the Omori formula is not expected to reasonably approximate aftershock numbers near origin time of a mainshock.
5. For several large mainshocks the recent inversions of slip time–space history exhibit temporal, spatial, and focal mechanism complexity of seismic moment release. I propose that this complexity be represented as an aftershock generating mechanism extended to a mainshock rupture process.
6. Therefore, in a final short-term approximation the earthquake process can be represented as a fractal assemblage of infinitesimal dislocations. What is usually called an individual earthquake is a tightly clustered group of subevents. An earthquake definition truly depends on the properties of the seismographic network and the methods of seismogram interpretation.

Acknowledgments

I thank D. D. Jackson and J. E. Vidale for stimulating discussions. Reviews by I. Main and an anonymous reviewer and suggestions by associate editor Götz Bokelmann have been very helpful in revising the manu-

script. Kathleen Jackson edited the final version. I appreciate partial support from the National Science Foundation through Grant EAR 00-01128, from CalTrans Grant 59A0363, and from the Southern California Earthquake Center (SCEC). SCEC is funded by NSF Cooperative Agreement EAR-0106924 and USGS Cooperative Agreement 02HQAG0008. SCEC Publication 750.

References

Abramowitz, M., and I. A. Stegun (1972). *Handbook of Mathematical Functions*, Dover, New York.

Aki, K., and P. Richards (1980). *Quantitative Seismology*, W. H. Freeman, New York.

Bak, P., and C. Tang (1989). Earthquakes as a self-organized critical phenomenon, *J. Geophys. Res.* **94,** 15,635–15,637.

Ben-Zion, Y., and C. G. Sammis (2002). Characterization of fault zones, *Pure Appl. Geophys.* **160,** 677–715.

Bilek, S. L., and T. Lay (1999). Rigidity variations with depth along interplate megathrust faults in subduction zones, *Nature* **400,** 443–446, 1673, doi 10.1038/22739.

Bunge, P., and J. Tromp (2003). Supercomputing moves to universities and makes possible new ways to organize computational research, *EOS* **84,** 30, 33.

Centroid Moment Tensor (CMT) Catalog. www.seismology.harvard.edu/CMT search.html (last accessed June 2004).

Chi, W. C., D. Dreger, and A. Kaverina (2001). Finite-source modeling of the 1999 Taiwan (Chi-Chi) earthquake derived from a dense strong-motion network, *Bull. Seism. Soc. Am.* **91,** 1144–1157.

Cohee, B. P., and G. C. Beroza (1994). Slip distribution of the 1992 Landers earthquake and its implications for earthquake source mechanics, *Bull. Seism. Soc. Am.* **84,** 692–712.

Console, R., and M. Murru (2001). A simple and testable model for earthquake clustering, *J. Geophys. Res.* **106,** 8699–8711.

Cowie, P. A., D. Sornette, and C. Vanneste (1995). Multifractal scaling properties of a growing fault population, *Geophys. J. Int.* **122,** 457–469.

Davis, S. D., and C. Frohlich (1991). Single-link cluster analysis of earthquake aftershocks: decay laws and regional variations, *J. Geophys. Res.* **96,** 6335–6350.

Delouis, B., D. Giardini, P. Lundgren, and J. Salichon (2002). Joint inversion of InSAR, GPS, teleseismic, and strong-motion data for the spatial and temporal distribution of earthquake slip: application to the 1999 Izmit mainshock, *Bull. Seism. Soc. Am.* **92,** 278–299.

Dieterich, J. (1994). A constitutive law for rate of earthquake production and its application to earthquake clustering, *J. Geophys. Res.* **99,** 2601–2618.

Dziewonski, A. M., T.-A. Chou, and J. H. Woodhouse (1981). Determination of earthquake source parameters from waveform data for studies of global and regional seismicity, *J. Geophys. Res.* **86,** 2825–2852.

Ebel, J. E., K.-P. Bonjer, and M. C. Oncescu (2000). Paleoseismicity: seismicity evidence for past large earthquakes, *Seism. Res. Lett.* **71,** no. 2, 283–294.

Ekström, G., A. M. Dziewonski, N. N. Maternovskaya, and M. Nettles (2003). Global seismicity of 2001: centroid-moment tensor solutions for 961 earthquakes, *Phys. Earth Planet. Interiors* **136,** no. 3–4, 165–185.

Felzer, K. R., T. W. Becker, R. E. Abercrombie, G. Ekström, and J. R. Rice (2002). Triggering of the 1999 M_w 7.1 Hector Mine earthquake by aftershocks of the 1992 M_w 7.3 Landers earthquake, *J. Geophys. Res.* **107,** no. B9, 2190, doi 10.1029/2001JB000911.

Field, E. H., D. D. Jackson, and J. F. Dolan (1999). A mutually consistent seismic-hazard source model for southern California, *Bull. Seism. Soc. Am.* **89,** 559–578.

Frankel, A. (1991). High-frequency spectral falloff of earthquakes, fractal dimension of complex rupture, *b* value, and the scaling of strength on faults, *J. Geophys. Res.* **96,** 6291–6302.

Frohlich, C., and S. D. Davis (1993). Teleseismic *b* values; or, much ado about 1.0, *J. Geophys. Res.* **98,** 631–644.

Gerstenberger, M. C., S. Wiemer, and L. M. Jones (2002). STEP: likelihood testing of an online time-dependent hazard mapping application (abstract), *EOS* **83,** no. 47, (Fall Meet. Suppl.), S12B-1195.

Gomberg, J., P. Bodin, and P. A. Reasenberg (2003). Observing earthquakes triggered in the near field by dynamic deformations, *Bull. Seism. Soc. Am.* **93,** 118–138.

Gutenberg, B., and C. F. Richter (1941). *Seismicity of the Earth*, Geol. Soc. Amer. Special Pap. **34,** 1–131.

Gutenberg, B., and C. F. Richter (1944). Frequency of earthquakes in California, *Bull. Seism. Soc. Am.* **34,** 185–188.

Habermann, R. E., W. R. McCann, and B. Perin (1993). Spatial seismicity variations along convergent plate boundaries, *Geophys. J. Int.* **85,** 43–68.

Heaton, T. H. (1990). Evidence for and implications of self-healing pulses of slip in earthquake rupture, *Phys. Earth Planet. Interiors* **64,** 1–20.

Helmstetter, A., and D. Sornette (2002). Subcritical and supercritical regimes in epidemic models of earthquake aftershocks, *J. Geophys. Res.* **107,** no. 10, 2237, 10.1029/2001JB001580.

Hileman, J. A., C. R. Allen, and J. M. Nordquist (1973). Seismicity of the southern California region, 1 January 1932 to 31 December 1972, Cal. Inst. Technology, Pasadena, California.

Houston, H. (2001). Influence of depth, focal mechanism, and tectonic setting on the shape and duration of earthquake source time functions, *J. Geophys. Res.* **106,** 11,137–11,150.

Hutton, L. K., and L. M. Jones (1993). Local magnitudes and apparent variations in seismicity rates in southern California, *Bull. Seism. Soc. Am.* **83,** 313–329.

Kagan, Y. Y. (1982). Stochastic model of earthquake fault geometry, *Geophys. J. R. Astr. Soc.* **71,** 659–691.

Kagan, Y. Y. (1990). Random stress and earthquake statistics: spatial dependence, *Geophys. J. Int.* **102,** 573–583.

Kagan, Y. Y. (1991a). Seismic moment distribution, *Geophys. J. Int.* **106,** 123–134.

Kagan, Y. Y. (1991b). Likelihood analysis of earthquake catalogues, *Geophys. J. Int.* **106,** 135–148.

Kagan, Y. Y. (2002). Aftershock zone scaling, *Bull. Seism. Soc. Am.* **92,** 641–655.

Kagan, Y. Y. (2003). Accuracy of modern global earthquake catalogs, *Phys. Earth Planet. Interiors* **135,** no. 2–3, 173–209.

Kagan, Y. Y., and L. Knopoff (1980). Dependence of seismicity on depth, *Bull. Seism. Soc. Am.* **70,** 1811–1822.

Kagan, Y. Y., and L. Knopoff (1981). Stochastic synthesis of earthquake catalogs, *J. Geophys. Res.* **86,** 2853–2862.

Kagan, Y. Y., and L. Knopoff (1987a). Random stress and earthquake statistics: time dependence, *Geophys. J. R. Astr. Soc.* **88,** 723–731.

Kagan, Y. Y., and L. Knopoff (1987b). Statistical short-term earthquake prediction, *Science* **236,** 1563–1567.

Kagan, Y. Y., and D. D. Jackson (2000). Probabilistic forecasting of earthquakes, *Geophys. J. Int.* **143,** 438–453.

Kaverina, A., D. Dreger, and E. Price (2002). The combined inversion of seismic and geodetic data for the source process of the 16 October 1999 M_w 7.1 Hector Mine, California, earthquake, *Bull. Seism. Soc. Am.* **91,** 1266–1280.

Kisslinger, C. (1996). Aftershocks and fault-zone properties, *Adv. Geophys.* **38,** 1–36.

Ma, K. F., J. Mori, S. J. Lee, and S. B. Yu (2001). Spatial and temporal distribution of slip for the 1999 Chi-Chi, Taiwan, earthquake, *Bull. Seism. Soc. Am.* **91,** 1069–1087.

Madariaga, R., and K. B. Olsen (2002). Earthquake dynamics, in *IASPEI Handbook of Earthquake and Engineering Seismology*, W. H. K. Lee, H. Kanamori, P. C. Jennings, and C. Kisslinger (Editors), Academic, New York, 175–194.

Main, I. G. (1996). Statistical physics, seismogenesis, and seismic hazard, *Rev. Geophys.* **34,** 433–462.

McGuire, J. J., L. Zhao, and T. H. Jordan (2001). Teleseismic inversion for

the second-degree moments of earthquake space-time distributions, *Geophys. J. Int.* **145,** 661–678.

Narteau, C., P. Shebalin, and M. Holschneider (2002). Temporal limits of the power law aftershock decay rate, *J. Geophys. Res.* **107,** ESE12, 2359, 10.1029/2002JB001868.

Nyffenegger, P., and C. Frohlich (2000). Aftershock occurrence rate decay properties for intermediate and deep earthquake sequences, *Geophys. Res. Lett.* **27,** 1215–1218.

Ogata, Y. (1983). Estimation of the parameters in the modified Omori formula for aftershock frequencies by the maximum likelihood procedure, *J. Physics Earth* **31,** 115–124.

Ogata, Y. (1988). Statistical models for earthquake occurrence and residual analysis for point processes, *J. Am. Stat. Assoc.* **83,** 9–27.

Ogata, Y. (1998). Space-time point-process models for earthquake occurrences, *Ann. Inst. Stat. Math.* **50,** no. 2, 379–402.

Ogata, Y. (1999). Seismicity analysis through point-process modeling: a review, *Pure Appl. Geophys.* **155,** 471–507.

Omori, F. (1894). On the after-shocks of earthquakes, *J. College Sci. Imp. Univ. Tokyo* **7,** 111–200.

Prudnikov, A. P., Yu. A. Brychkov, and O. I. Marichev (1992). *Integrals and Series*, Vol. 3, Gordon and Breach, New York.

Reasenberg, P. A., and L. M. Jones (1989). Earthquake hazard after a mainshock in California, *Science* **243,** 1173–1176.

Reasenberg, P. A., and L. M. Jones (1994). Earthquake aftershocks: update, *Science* **265,** 1251–1252.

Richter, C. F. (1955). Foreshocks and aftershocks, in Earthquakes in Kern County, California during 1952, *Calif. Div. Mines Bull.* **171,** 177–197.

Rubin, A. M. (2002). Aftershocks of microearthquakes as probes of the mechanics of rupture, *J. Geophys. Res.* **107,** no. B7, ESE3, 2142, 10.1029/2001JB000496.

Sato, H., and M. C. Fehler (1998). *Seismic Wave Propagation and Scattering in the Heterogeneous Earth*, AIP, New York, 308 pp.

Sornette, D. (2003). *Critical Phenomena in Natural Sciences: Chaos, Fractals, Self-Organization, and Disorder—Concepts and Tools*, Second Ed., Springer, New York, 528 pp.

Sornette, D., and A. Helmstetter (2002). Occurrence of finite-time singularities in epidemic models of rupture, earthquakes, and starquakes, *Phys. Rev. Lett.* **8915,** U227–U230, Art. no. 158501.

Tanioka, Y., and L. Ruff (1997). Source time functions, *Seism. Res. Lett.* **68,** no. 3, 386–397.

Thio, H. K., and H. Kanamori (1996). Source complexity of the 1994 Northridge earthquake and its relation to aftershock mechanisms, *Bull. Seism. Soc. Am.* **86,** S84–S92.

Uchaikin, V. V., and V. M. Zolotarev (1999). *Chance and Stability: Stable Distributions and Their Applications*, VSP, Utrecht, the Netherlands, 570 pp.

Utsu, T. (1961). A statistical study on the occurrence of aftershocks, *Geophys. Mag.* **30,** 521–605.

Utsu, T. (1969). Aftershocks and earthquake statistics (I): some parameters which characterize an aftershock sequence and their interrelations, *J. Fac. Sci. Hokkaido Univ. Japan Ser. VII* **3,** 129–195.

Utsu, T. (1999). Representation and analysis of the earthquake size distribution: a historical review and some new approaches, *Pure Appl. Geophys.* **155,** 509–535.

Utsu, T. (2002). Statistical features of seismicity, in *IASPEI Handbook of Earthquake and Engineering Seismology*, W. H. K. Lee, H. Kanamori, P. C. Jennings, and C. Kisslinger (Editors), Academic, New York, 719–732.

Utsu, T., Y. Ogata, and R. S. Matsu'ura (1995). The centenary of the Omori formula for a decay law of aftershock activity, *J. Phys. Earth* **43,** 1–33.

Vidale, J. E., E. S. Cochran, H. Kanamori, and R. W. Clayton (2003). After the lightning and before the thunder: non-Omori behavior of early aftershocks? (abstract), *EOS* **84,** no. 46 (Fall Meet. Suppl.), S31A-08.

Wald, D. J., and T. H. Heaton (1994). Spatial and temporal distribution of slip for the 1992 Landers, California, earthquake, *Bull. Seism. Soc. Am.* **84,** 668–691.

Wald, D. J., T. H. Heaton, and K. W. Hudnut (1996). The slip history of the 1994 Northridge, California, earthquake determined from strong-motion, teleseismic, GPS, and leveling data, *Bull. Seism. Soc. Am.* **86,** S49–S70.

Wald, D. J., D. V. Helmberger, and T. H. Heaton (1991). Rupture model of the 1989 Loma-Prieta earthquake from the inversion of strong-motion and broad-band teleseismic data, *Bull. Seism. Soc. Am.* **81,** 1540–1572.

Waldhauser, F., and W. L. Ellsworth (2000). A double-difference earthquake location algorithm: method and application to the northern Hayward fault, California, *Bull. Seism. Soc. Am.* **90,** 1353–1368.

Wiemer, S., and K. Katsumata (1999). Spatial variability of seismicity parameters in aftershock zones, *J. Geophys. Res.* **104,** 13,135–13,151.

Wiemer, S., and M. Wyss (2000). Minimum magnitude of completeness in earthquake catalogs: examples from Alaska, the western United States, and Japan, *Bull. Seism. Soc. Am.* **90,** 859–869.

Wiemer, S., M. Gerstenberger, and E. Hauksson (2002). Properties of the aftershock sequence of the 1999 M_w 7.1 Hector Mine earthquake: implications for aftershock hazard, *Bull. Seism. Soc. Am.* **92,** 1227–1240.

Willemann, R. J. (1999a). Regional thresholds of the ISC bulletin, *Seism. Res. Lett.* **70,** no. 3, 313–321.

Willemann, R. J. (1999b). Errata, *Seism. Res. Lett.* **70,** no. 5, 529.

Wolfram, S. (1999). *The Mathematica Book*, Fourth Ed., Cambridge U Press, New York.

Zeng, Y. H., and J. G. Anderson (1996). A composite source model of the 1994 Northridge earthquake using genetic algorithms, *Bull. Seism. Soc. Am.* **86,** S71–S83.

Zolotarev, V. M. (1986). *One-Dimensional Stable Distributions*, American Mathematical Society, Providence, R.I.

Department of Earth and Space Sciences
University of California
Los Angeles, California 90095-1567
ykagan@ucla.edu

Manuscript received 21 May 2003.